

NASA Contractor Report 178145

NASA-CR-178145
19860022226

**Study on Effects of Powder and Flake
Chemistry and Morphology on the Properties of
Al-Cu-Mg-X-X-X Powder Metallurgy Advanced
Aluminum Alloys – Final Report**

P. J. Meschter, R. J. Lederich, and J. E. O'Neal

McDonnell Douglas Research Laboratories
St. Louis, Missouri

Contract NAS1-17107
August 1986

LIBRARY COPY

SEP 25 1986

LANGLEY RESEARCH CENTER
LIBRARY, NASA
HAMPTON, VIRGINIA



National Aeronautics and
Space Administration

Langley Research Center
Hampton, Virginia 23665-5225



NF00184

NASA Contractor Report 178145

**Study on Effects of Powder and Flake
Chemistry and Morphology on the Properties of
Al-Cu-Mg-X-X-X Powder Metallurgy Advanced
Aluminum Alloys – Final Report**

P. J. Meschter, R. J. Lederich, and J. E. O'Neal

McDonnell Douglas Research Laboratories
St. Louis, Missouri

Contract NAS1-17107
August 1986

NASA

National Aeronautics and
Space Administration

Langley Research Center
Hampton, Virginia 23665-5225

N86-31698 #

PREFACE

This report presents the results of research performed from 21 September 1984 through 31 March 1986 by the McDonnell Douglas Research Laboratories under the National Aeronautics and Space Administration Contract NAS1-17107 entitled "Study of Effects of Powder and Flake Chemistry and Morphology on the Properties of Al-Cu-Mg-X-X-X Powder Metallurgy Advanced Aluminum Alloys." The objectives of the modification reported on here were (1) to develop RSP Al-3Cu-2Li-1Mg-0.2Zr alloys as high-strength, low-density substitutes for titanium alloys and commercial 2XXX aluminum alloys for service to at least 150°C, and (2) to develop RSP Al-4Li-Cu-Mg-Zr alloys as low-density substitutes for high-strength commercial 7XXX alloys in ambient-temperature applications. The results provide an improved fundamental understanding of microstructure/property relationships in these alloy classes and allow a preliminary evaluation of their potential for the intended applications.

The research was performed in the Solid State Sciences Department, managed by Dr. C. R. Whitsett. The principal investigator was Dr. P. J. Meschter; co-investigators were Mr. R. J. Lederich and Mr. J. E. O'Neal. The technical manager was Mr. W. Barry Lisagor, NASA--Langley Research Center.

CONTENTS

	Page
1. INTRODUCTION.....	1
2. RESEARCH OBJECTIVES AND APPROACH.....	3
2.1 Objectives.....	3
2.2 Selection of Alloy Compositions.....	3
2.2.1 High-Strength Alloys for 150°C Applications.....	3
2.2.2 Low-Density Alloys for Ambient-Temperature Applications.....	6
3. EXPERIMENTAL PROCEDURE.....	8
3.1 Particulate Production, Consolidation, and Post- Consolidation Processing.....	8
3.2 Microstructures and Properties of Consolidated Forms.....	9
3.2.1 Microstructure and Density.....	9
3.2.2 Mechanical Properties.....	9
4. TASK 5: HIGH-STRENGTH RSP Al-3Cu-2Li-1Mg-0.2Zr ALLOYS FOR AMBIENT AND ELEVATED-TEMPERATURE SERVICE.....	11
4.1 Evaluation of Dispersoid-Forming Additives.....	11
4.2 Alloy Composition.....	12
4.3 Microstructure.....	18
4.3.1 Evaluation of Inclusions.....	18
4.3.2 As-Extruded Condition.....	20
4.3.3 Solution-Treated Condition.....	22
4.3.4 Aged Conditions.....	25
4.4 Properties.....	29
4.4.1 Density and Elastic Modulus.....	29
4.4.2 Mechanical Properties.....	29
4.4.3 Fracture Toughness.....	35
4.4.4 Fatigue-Crack-Growth Rate.....	37
4.4.5 Creep Resistance.....	38
4.4.6 Corrosion Resistance.....	38
4.5 Microstructure/Properties Correlation.....	39
5. TASK 6: LOW-DENSITY Al-4Li-Cu-Mg-Zr ALLOYS FOR AMBIENT- TEMPERATURE APPLICATIONS.....	45
5.1 Alloy Composition.....	45
5.2 Microstructure.....	45
5.2.1 Evaluation of Inclusions.....	45
5.2.2 As-Extruded Condition.....	47
5.2.3 Solution-Treated Condition.....	47
5.2.4 Aged Condition.....	50

CONTENTS (Continued)

	<u>Page</u>
5.3 Properties.....	54
5.3.1 Density and Elastic Modulus.....	54
5.3.2 Mechanical Properties.....	54
5.3.3 Fracture Toughness.....	55
5.3.4 Fatigue-Crack-Growth Rate.....	56
5.3.5 Corrosion Resistance.....	57
5.4 Microstructure/Properties Correlation.....	57
6. CONCLUSIONS.....	59
7. REFERENCES.....	61

LIST OF ILLUSTRATIONS

<u>Figure</u>	<u>Page</u>
1. Typical phase diagrams of (a) eutectic and (b) peritectic dispersoid-forming Al-base binary systems.....	5
2. Transmission electron micrographs of roller-quenched flakes: (a) Al-1.8Cr, (b) Al-3.9Y, (c) Al-4.5Ce, and (d) Al-6.5Er.....	13
3. Transmission electron micrographs of roller-quenched Al-1.8Cr flakes heat treated for 1 hr at (a) 400, (b) 500, (c) 550, and (d) 600°C.....	14
4. Transmission electron micrographs of roller-quenched Al-3.9Y flakes heat treated for 1 hr at (a) 400, (b) 500, (c) 550, and (d) 600°C.....	15
5. Transmission electron micrographs of roller-quenched Al-4.5Ce flakes heat treated for 1 hr at (a) 400, (b) 500, (c) 550, and (d) 600°C.....	16
6. Transmission electron micrographs of roller-quenched Al-6.5Er flakes heat treated for 1 hr at (a) 400, (b) 500, (c) 550, and (d) 600°C.....	17
7. Optical photomicrographs of unetched samples of (a) Al-3Cu-2Li-1Mg-0.2Zr and (b) Al-3Cu-2Li-1Mg-1Fe-1Ni-0.2Zr extrusions, solution-treated 560°C/1 hr.....	19
8. Optical photomicrographs of as-received extrusions of (a) Al-3Cu-2Li-1Mg-0.2Zr, (b) Al-3Cu-2Li-1Mg-1Fe-1Ni-0.2Zr, and (c) Al-3Cu-2Li-1Mg-1.6Cr-0.2Zr.....	21
9. Optical photomicrographs of (a) Al-3Cu-2Li-1Mg-0.2Zr, (b) Al-3Cu-2Li-1Mg-1Fe-1Ni-0.2Zr, and (c) Al-3Cu-1Li-1Mg-1.6Cr-0.2Zr extrusions, solution-treated at 560°C for 1 hr.....	23
10. Transmission electron photomicrographs of 560°C solution-treated and quenched (a) Al-3Cu-2Li-1Mg-0.2Zr, (b) Al-3Cu-2Li-1Mg-1Fe-1Ni-0.2Zr, and (c) Al-3Cu-2Li-1Mg-1.6Cr-0.2Zr.....	24
11. Transmission electron photomicrographs of 560°C solution-treated and aged RSP Al-3Cu-2Li-1Mg-0.2Zr: (a),(b) T6 temper, and (c),(d) T8 temper.....	26
12. Transmission electron photomicrographs of 560°C solution-treated and aged RSP Al-3Cu-2Li-1Mg-1Fe-1Ni-0.2Zr: (a),(b) T6 temper, and (c),(d) T8 temper.....	27
13. Transmission electron photomicrographs of 560°C solution-treated and aged RSP Al-3Cu-2Li-1Mg-1.6Cr-0.2Zr: (a),(b) T6 temper, and (c),(d) T8 temper.....	28

LIST OF ILLUSTRATIONS (Continued)

<u>Figure</u>	<u>Page</u>
14. Variation with temperature of the yield stress after 100 hr exposure at temperature of Al-3Cu-2Li-1Mg-0.2Zr, Al-3Cu-2Li-1Mg-1Fe-1Ni-0.2Zr and Al-3Cu-2Li-1Mg-1.6Cr-0.2Zr. Original temper T6. 2124-T851 plate (reference 16).....	33
15. Variation with temperature of the ultimate tensile stress after 100 hr exposure at temperature of Al-3Cu-2Li-1Mg-0.2Zr, Al-3Cu-2Li-1Mg-1Fe-1Ni-0.2Zr and Al-3Cu-2Li-1Mg-1.6Cr-0.2Zr. Original temper T6. 2124-T851 plate (reference 16).....	34
16. Variation with temperature of the ductility after 100 hr exposure at temperature of Al-3Cu-2Li-1Mg-0.2Zr, Al-3Cu-2Li-1Mg-1Fe-1Ni-0.2Zr and Al-3Cu-2Li-1Mg-1.6Cr-0.2Zr. Original temper T6. 2124-T851 plate (reference 16).....	35
17. Variation with temperature of the yield stress after 100 hr exposure at temperature of Al-3Cu-2Li-1Mg-0.2Zr, Al-3Cu-2Li-1Mg-1Fe-1Ni-0.2Zr and Al-3Cu-2Li-1Mg-1.6Cr-0.2Zr. Original temper T8. 2124-T851 plate (reference 16).....	36
18. Variation with temperature of the ultimate tensile stress after 100 hr exposure at temperature of Al-3Cu-2Li-1Mg-0.2Zr, Al-3Cu-2Li-1Mg-1Fe-1Ni-0.2Zr, and Al-3Cu-2Li-1Mg-1.6Cr-0.2Zr. Original temper T8. 2124-T851 plate (reference 16).....	37
19. Variation with temperature of the ductility after 100 hr exposure at temperature of Al-3Cu-2Li-1Mg-0.2Zr, Al-3Cu-2Li-1Mg-1Fe-1Ni-0.2Zr, and Al-3Cu-2Li-1Mg-1.6Cr-0.2Zr. Original temper T8. 2124-T851 plate (reference 16).....	38
20. Variation with temperature of the density-normalized yield stress after 100 hr exposure at temperature of Al-3Cu-2Li-1Mg-0.2Zr-T6, Al-3Cu-2Li-1Mg-1Fe-1Ni-0.2Zr-T6, Al-3Cu-2Li-1Mg-1.6Cr-0.2Zr-T6, 2124-T851 plate (reference 16), Ti-6Al-4V, mill annealed (reference 15), and Ti-6Al-4V, solution-treated and aged (reference 15).....	39
21. Variation with temperature of the density-normalized yield stress after 100 hr exposure at temperature of Al-3Cu-2Li-1Mg-0.2Zr-T8, Al-3Cu-2Li-1Mg-1Fe-1Ni-0.2Zr-T8, Al-3Cu-2Li-1Mg-1.6Cr-0.2Zr-T8, 2124-T851 plate (reference 16), Ti-6Al-4V, mill annealed (reference 15), and Ti-6Al-4V, solution-treated and aged (reference 15).....	40
22. FCGR results on Al-3Cu-2Li-1Mg-1.6Cr-0.2Zr, T8 temper: LT orientation, TL orientation, and typical results for 2124-T851 (reference 16).....	41
23. 150°C creep-test results for Al-3Cu-2Li-1Mg-1.6Cr-0.2Zr-T8 and typical results for 2124-T851 (reference 16).....	42

LIST OF ILLUSTRATIONS (Continued)

<u>Figure</u>	<u>Page</u>
24. Optical photomicrographs of unetched samples of (a) Al-4Li-1Cu-1Mg-0.2Zr and (b) Al-4Li-0.5Cu-1.5Mg-0.2Zr extrusions, solution-treated 560°C/1 hr.....	46
25. Optical photomicrographs of as-received extrusions of (a) Al-4Li-1Cu-1Mg-0.2Zr, (b) Al-4Li-0.5Cu-1.5Mg-0.2Zr, and (c) Al-4Li-1.5Cu-0.5Mg-0.2Zr.....	48
26. Optical photomicrographs of (a) Al-4Li-1Cu-1Mg-0.2Zr, (b) Al-4Li-0.5Cu-1.5Mg-0.2Zr, and (c) Al-4Li-1.5Cu-0.5Mg-0.2Zr extrusions, solution-treated at 560°C for 1 hr.....	49
27. Transmission electron photomicrographs of 560°C solution-treated and quenched (a), (b) Al-4Li-1Cu-1Mg-0.2Zr, (c), (d) Al-4Li-0.5Cu-1.5Mg-0.2Zr and (e), (f) Al-4Li-1.5Cu-0.5Mg-0.2Zr.....	51
28. Transmission electron photomicrographs of RSP Al-4Li alloys, solution-treated 560°C/1 hr and aged 160°C/48 hr (T6), or solution-treated 560°C/1 hr, stretched 2%, and aged 160°C/48 hr (T8). (a), (b) Al-4Li-1Cu-1Mg-0.2Zr; (a) T6, (b) T8; (c), (d) Al-4Li-0.5Cu-1.5Mg-0.2Zr; (c) T6, (d) T8; (e)-(h) Al-4Li-1.5Cu-0.5Mg-0.2Zr; (e), (f) T6; (g), (h) T8.....	52
28. (Continued) Transmission electron photomicrographs of RSP Al-4Li alloys, solution-treated 560°C/1 hr and aged 160°C/48 hr (T6), or solution-treated 560°C/1 hr, stretched 2%, and aged 160°C/48 hr (T8). (a), (b) Al-4Li-1Cu-1Mg-0.2Zr; (a) T6, (b) T8; (c), (d) Al-4Li-0.5Cu-1.5Mg-0.2Zr; (c) T6, (d) T8; (e)-(h) Al-4Li-1.5Cu-0.5Mg-0.2Zr; (e), (f) T6; (g), (h) T8.....	53
29. FCGR results on Al-4Li-1Cu-1Mg-0.2Zr, T851 temper: LT orientation, TL orientation, and typical results for 7075-T651 (reference 16).....	57

LIST OF TABLES

<u>Table</u>	<u>Page</u>
1. Density-Normalized Yield Stresses of Elevated-Temperature Al and Ti Alloys.....	4
2. Mechanical Properties of RSP Al-4Li Alloys.....	7
3. Compositions of RSP Al-3Cu-2Li-1Mg-0.2Zr Alloys.....	18
4. Constituent and Dispersed Phases in As-Extruded and Solution-Treated Al-3Cu-2Li-1Mg-0.2Zr Alloys.....	20
5. Mass Densities and Elastic Moduli of Al-3Cu-2Li-1Mg-0.2Zr Alloys..	30
6. Ambient-Temperature Longitudinal Mechanical Properties of Peak-Aged Al-3Cu-2Li-1Mg-0.2Zr Alloys.....	30
7. Ambient-Temperature Long-Transverse Mechanical Properties of Al-3Cu-2Li-1Mg-0.2Zr Alloys.....	31
8. Longitudinal Mechanical Properties of Al-3Cu-2Li-1Mg-0.2Zr Alloys in the T3 and Underaged T8 Tempers.....	31
9. Ambient-Temperature Compressive Yield Stresses of Al-3Cu-2Li-1Mg-0.2Zr Alloys.....	32
10. Compositions of RSP Al-4Li-Cu-Mg-Zr Alloys.....	45
11. Constituent and Dispersed Phases in As-Extruded and Solution-Treated Al-4Li-Cu-Mg-Zr Alloys.....	47
12. Mass Densities of Al-4Li-Cu-Mg-Zr Alloys.....	54
13. Ambient-Temperature Mechanical Properties of Peak-Aged Al-4Li-Cu-Mg-0.2Zr Alloys.....	55
14. Ambient-Temperature Long-Transverse Mechanical Properties of Peak-Aged Al-4Li-Cu-Mg-0.2Zr Alloys.....	56
15. Ambient-Temperature Compressive Yield Stresses of RSP Al-4Li-Cu-Mg-0.2Zr Alloys.....	56

1. INTRODUCTION

The final report on the first phase of this study (1), as well as numerous studies at MDRL (2-10) and elsewhere (11-13), have shown that rapid solidification processed (RSP) aluminum-lithium alloys have attractive combinations of low density, high modulus, and high strength, while possessing reasonable ductilities. Although it was initially considered that RSP would be required for commercialization of all Al-Li alloys, advances in ingot-casting technology have enabled alloys containing up to 2.5 wt% Li to be produced by conventional ingot-metallurgical (I/M) methods. Development of the I/M alloys 2090 (Al-2.9Cu-2.2Li-0.1Zr) and 8091 (Al-2.0Cu-2.5Li-0.7Mg-0.1Zr) has rendered superfluous the development of RSP Al-Li alloys containing ≤ 3 wt% Li, since production and consolidation of RSP particulates entail higher costs than ingot-metallurgical processing.

The emphasis in RSP Al-Li alloy research has shifted to compositions which can currently be produced only by RSP and which potentially have properties combinations uniquely suited to specific applications. Improved properties are achieved through RSP by (a) adding Li in concentrations which cannot be homogeneously incorporated by I/M processing, and (b) strengthening by fine, incoherent dispersoids containing sparsely soluble elements such as Ti, V, Cr, Mn, Fe, Co, Ni, Ge, Y, Nb, Mo, Ta, W, or rare earths. These dispersoids cannot be sufficiently refined in ingot casting to significantly improve strength. Since the dispersion-strengthening contribution is essentially temperature-independent, RSP dispersoid-containing alloys have unique potential for elevated-temperature applications. The ability of RSP to produce Al-Li alloys with unique properties by increasing the Li concentration above 3 wt% or by incorporating controlled volume fractions of dispersoids must be evaluated before these promising new alloys can be commercially exploited.

Previous research on RSP Al-Li alloys has concentrated on alloys with $\leq 10\%$ reductions in density relative to commercial 2XXX and 7XXX alloys. Alloys with ≥ 4 wt% Li and $\geq 14\%$ density reductions can be produced only by RSP and have high payoffs for ambient-temperature structural applications. Research on this alloy class (10,14) has established that RSP Al-4Li-Zr alloys have attractive mechanical properties, but the effect of additions of quater-

nary and quinary alloying elements such as Mg and Cu has not been systematically explored. The effect of the Cu:Mg ratio on the properties of RSP Al-4Li-Cu-Mg-Zr alloys was determined in the present investigation with a view towards optimizing the properties of Al high-Li alloys.

Replacement of titanium alloys such as Ti-6Al-4V by aluminum alloys in structural applications requiring 150°C (300°F) service would allow significant weight reductions in supersonic aircraft. An RSP Al alloy with a significant Li concentration and a controlled volume fraction of fine dispersoids would have an attractive combination of low density and high specific strength at the service temperature. In this investigation, the elevated-temperature properties of baseline and dispersoid-containing RSP Al-3Cu-2Li-1Mg-0.2Zr alloys were determined with the goal of developing such a "combined-properties" alloy.

2. RESEARCH OBJECTIVES AND APPROACH

In the first phase of this study (1), the effects of particulate cooling rate and shape, oxide film formation and break-up, phase relationships, and recrystallization and texturing on the properties of RSP Al alloys for ambient- and elevated-temperature applications were investigated. In the second phase reported here, the effects of high Li concentrations on ambient-temperature properties and of a combination of Li and dispersoid-forming elements on elevated-temperature properties of RSP Al-Li alloys were explored.

2.1 Objectives

1. Develop RSP Al-3Cu-2Li-1Mg-0.2Zr alloys for service to at least 150°C (300°F) which have strength/density ratios superior to those of Ti-6Al-4V and commercial 2XXX-series Al alloys normally used in elevated-temperature service. These RSP alloys will contain controlled Li and dispersoid-forming element concentrations to combine the density reduction imparted by Li with the temperature-insensitive strengthening afforded by the dispersoids.
2. Develop Al-4Li-Cu-Mg-0.2Zr alloys as low-density substitutes for high-strength commercial 7XXX alloys in ambient-temperature applications.

This research was divided into two tasks, as follows:

Task 5: High-Strength RSP Al-3Cu-2Li-1Mg-0.2Zr Alloys for Ambient- and Elevated-Temperature Service, and

Task 6: Low-Density RSP Al-4Li-Cu-Mg-Zr Alloys for Ambient-Temperature Applications.

2.2 Selection of Alloy Compositions

2.2.1 High-Strength Alloys for 150°C Applications

Density-normalized yield stresses of aluminum and titanium alloys commonly used in 150°C applications are listed in Table 1. The specific yield stress of the strongest commercial aluminum alloy is seen to be 19% lower than that of mill-annealed Ti-6Al-4V at ambient temperature and 14% lower at 150°C.

TABLE 1. DENSITY-NORMALIZED YIELD STRESSES OF ELEVATED-TEMPERATURE Al AND Ti ALLOYS.

Alloy	Temper	Density (g/cm ³)	25°C		150°C		Ref.
			Yield stress (MPa)	Yield stress/ density ratio (MPa cm ³ g ⁻¹)	Yield stress (MPa)	Yield stress/ density ratio (MPa cm ³ g ⁻¹)	
Ti-6Al-4V	Mill annealed	4.43	885	200	735	166	15
Ti-6Al-4V	Solution-treated and aged	4.43	1040	235	880	199	15
2024-Al	T851	2.75	448	163	338	123	16
2124-Al	T851	2.77	450	162	395	143	16
2219-Al	T851	2.84	345	121	276	97	16
2618-Al	T61	2.76	372	135	303	110	16
RSP	{	2.60	517	199	—	—	17
Al-3Cu-2Li-1Mg-0.2Zr							
		2.60	578	222	—	—	17

GP61-0435-29-R

Relative to solution-treated and aged Ti-6Al-4V, the shortfall in specific strength is 31% at ambient temperature and 28% at 150°C.

The specific strength of aluminum alloys can be increased by decreasing their density, increasing their strength, or both. The density of aluminum is decreased by about 3% for each wt% Li added, so that a 2% Li addition yields a 6-7% increase in specific strength by density reduction alone. Several I/M and RSP Al-Li-Cu-Mg-Zr alloys have high ambient-temperature strengths. For instance, RSP Al-3Cu-2Li-1Mg-0.2Zr (17) has density-normalized yield stresses in the T6 and T8 conditions which are approximately equal to those of Ti-6Al-4V in the mill-annealed and solution-treated-and-aged conditions, respectively. Based on its high strength and ductilities ranging from 5 to 8%, RSP Al-3Cu-2Li-1Mg-0.2Zr was chosen as the baseline alloy for Task 5 of this investigation.

Dispersoid-forming additions to aluminum fall into eutectic- and peritectic-forming groups, as shown in Figure 1. The T_0 line, along which Gibbs energies of liquid and solid of the same composition are equal, represents the maximum temperature for segregationless solidification. This line

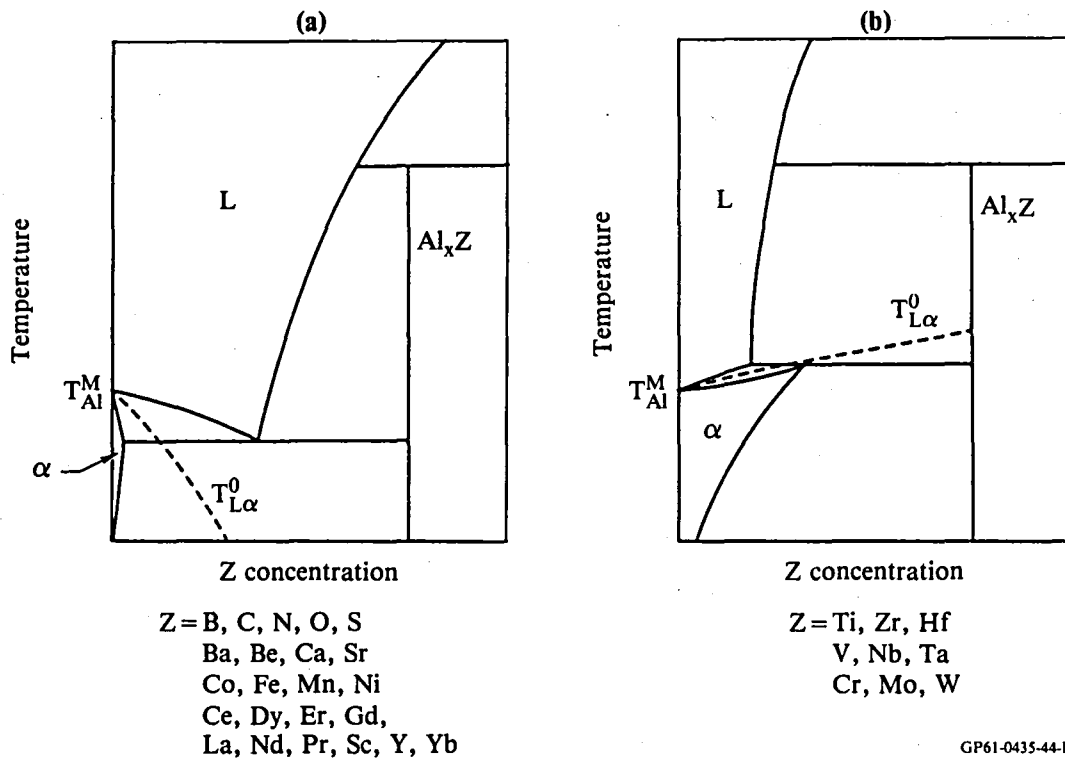


Figure 1. Typical phase diagrams of (a) eutectic and (b) peritectic dispersoid-forming Al-base binary systems.

falls with increasing solute concentration in eutectic systems (Figure 1a), but rises with increasing solute concentration in peritectic systems (Figure 1b). A large undercooling is required to form a metastable solid solution in a eutectic system; therefore, dispersoids in these systems tend to be formed upon solidification even at the high rates typical of RSP. It was shown (1) that Al_9FeNi dispersoids formed during RSP had sizes and spacings after heat treatment which were fixed by the solidification cell size and thus indirectly by the solidification rate. Dispersoid sizes and shapes in eutectic-forming systems are thus not amenable to modification by post-solidification processing and heat treatment.

In peritectic-forming systems, the relatively small undercooling required to form a metastable solid solution is readily attained upon rapid solidification, and segregation can be avoided. The dispersoids can then be precipitated, and their size and spacing controlled, during consolidation processing or heat treatment. Thus, it may be possible to form finer, more closely spaced dispersoids in peritectic-forming systems than in eutectic-forming systems.

For this investigation, one conventional and one novel dispersoid-forming system were chosen as additives to Al-3Cu-2Li-1Mg-0.2Zr. Based on previous experience, 1Fe + 1Ni was selected as the conventional system. This addition forms approximately 5 vol% Al₉FeNi dispersoids upon solidification. The novel system selected was based on a preliminary study of the peritectic-forming element Cr and the eutectic-forming elements Y, Ce, and Er. Cr was selected because the 1.8 wt% Cr required to yield 5 vol% Al₇Cr dispersoids could be readily dissolved in molten aluminum at a 100°C superheat. Other peritectic-forming elements such as V, and Mo have limited liquid solubilities in Al and would require much larger superheats to dissolve sufficient quantities for 5 vol% dispersoids. Y, Ce, and Er were selected because there is little or no experience with these additives, and because it has been shown (3,4) that more conventional additives such as Co and Mn do not produce finer dispersoids than [Fe + Ni].

2.2.2 Low-Density Alloys for Ambient-Temperature Applications

RSP Al-(4-5)Li alloys have been explored under the McDonnell Douglas Corporation Independent Research and Development (IRAD) program as low-density substitutes for 7XXX alloys (10). Al-4Li alloys have typical densities of 2.40-2.44 g/cm³ and Al-5Li alloys have typical densities of 2.33-2.36 g/cm³; these alloys are less dense than 7XXX-Al alloys by 13-14% and 16-17%, respectively. Retention of adequate ductility in these alloys requires \leq 5 vol% undissolved constituent phases such as δ (AlLi) or T₂ (Al₅Li₃Cu) (10). This condition cannot be met in Al-5Li alloys or in Al-4Li alloys with > 1 wt% added Cu or Mg. Mechanical properties of RSP Al-4Li alloys are listed in Table 2. Yield stresses of Al-4Li-Cu-Zr and Al-4Li-Mg-Zr alloys are comparable to that of 7050-Al plate in the T76511 temper. The ductility of Al-4Li-1Mg-0.2Zr is superior to that of Al-4Li-1Cu-0.2Zr, but the ductilities of Al-4Li alloys generally must be increased by at least 2-3% to satisfy conservative design criteria.

Previous research on RSP Al-Li-Cu-Zr, Al-Li-Mg-Zr, and Al-Li-Cu-Mg-Zr alloys (7,18) has shown that the strength and ductility of such alloys is strongly influenced not only by the total [Li + Cu + Mg] concentration, but also by the balance among Li, Cu, and Mg concentrations. Since this balance has not been explored for Al-4Li alloys, Al-4Li-1.5Cu-0.5Mg-0.2Zr, Al-4Li-1Cu-

**TABLE 2. MECHANICAL PROPERTIES OF RSP
Al-4Li ALLOYS.**

Alloy	Temper	Yield stress (MPa)	Ultimate tensile stress (MPa)	Elongation (%)
Al-4Li-0.2Zr	T6	449	509	6.0
Al-4Li-1Cu-0.2Zr	T6	473	510	3.8
	T8	496	530	2.8
Al-4Li-1Mg-0.2Zr	T6	468	514	4.9
	T8	470	524	4.2
7075	T651	503	573	11
7050	T76511	476	545	7

GP61-0435-30-R

1Mg-0.2Zr, and Al-4Li-0.5Cu-1.5Mg-0.2Zr were selected for investigation under this contract program; the selected compositions have Cu:Mg ratios of 3:1, 1:1, and 1:3, respectively.

3. EXPERIMENTAL PROCEDURE

3.1 Particulate Production, Consolidation, and Post-Consolidation Processing

Rapidly solidified Al-Cr, Al-Y, Al-Ce, and Al-Er flakes for selection of the novel dispersoid-forming additive to Al-3Cu-2Li-1Mg-0.2Zr alloys were produced by twin-roller quenching at MDRL. This method produces flakes approximately 125- μ m thick which are convenient for rapid heat treatment and for examination by transmission electron microscopy. The solidification rate of roller-quenched flakes is approximately 4×10^5 K/s (1). This process was described in the previous report (1) and elsewhere (7).

Six batches of spherical powder of the desired Al-3Cu-2Li-1Mg-0.2Zr and Al-4Li-Cu-Mg-0.2Zr compositions were produced by vacuum atomization at Homogeneous Metals, Inc. (HMI), Clayville, NY. The procedure was similar to that described in the previous report (1) except that the melt mass was increased from 8 to 16 kg, and all the powder of each composition was produced in a single run. Yields of -80 mesh powder ranged from 9.5 to 14.1 kg. Vacuum-atomized Al-Li powders were extensively characterized in the previous report and were found to have a geometric mean particle diameter of approximately 40 μ m and a mean solidification rate of $\sim 10^4$ K/s. The powders were packaged under inert-gas cover for shipment to the consolidation vendor.

The powders were consolidated to rectangular extrusions at the Kaiser Center for Technology, Pleasanton, CA. Since HMI had observed that the Al-4Li powders were significantly more reactive with air than the Al-3Li powders produced previously, as-received powders were handled under inert gas cover. The powders were loaded into rubber containers and cold isostatically pressed to approximately 70%-dense green compacts. The compacts were canned and degassed using Kaiser's proprietary depurative degassing process at temperatures up to 510°C (950°F) and then hot pressed into billets of 100% density at 510°C. The billets were decanned and extruded at 400°C to 1.27 x 5.72-cm rectangular-bar extrusions at an extrusion ratio of 19:1.

Previous experience (1,10,17,18) has established 560°C as the highest solution-treatment temperature attainable for both alloy types without incipient melting. The combined [Li + Cu + Mg] concentration in alloys for both tasks 5 and 6 is slightly in excess of the equilibrium solubility limit at 560°C. Solution-treating at lower temperatures retains larger volume fractions of undissolved constituent phases, which lowers ductility (10), and

reduces volume fractions of precipitated phases, thus lowering strength. Accordingly, we chose a temperature of 560°C for solution-treatment of all alloys.

We chose a uniform aging temperature of 160°C for all alloys. This temperature was chosen as a compromise between production of large volume fractions of precipitated phases, which is promoted by low aging temperatures, and decreased aging time, which is promoted by high aging temperatures. The 160°C aging curves of Al-4Li alloys show flat maxima between 16 and 64 hr aging time (10), and 48-64 hr was found to be the optimal aging time range for the Al-3Cu-2Li-1Mg-0.2Zr alloys.

3.2 Microstructures and Properties of Consolidated Forms

3.2.1 Microstructure and Density

Optical micrographs of all alloys were obtained in the as-extruded and solution-treated conditions to characterize the grain structures and the sizes, shapes, and distributions of constituent particles, oxides, and inclusions. Transmission electron micrographs of all alloys were obtained in the solution-treated, T6 (peak-aged), and T8 (stretched and peak-aged) tempers to characterize subgrain diameters and sizes and distributions of precipitated phases. Direct microstructural observations were supplemented by x-ray diffraction patterns to identify constituent and precipitated phases present as a function of alloy composition and heat treatment. Mass densities of all alloys were determined by the two-liquid method (1,19), which is accurate to $\pm 0.002 \text{ g/cm}^3$.

3.2.2 Mechanical Properties

The elastic moduli, yield stresses, ultimate tensile stresses, and ductilities of alloy extrusions in various tempers and orientations were determined for the Al-3Cu-2Li-1Mg-0.2Zr alloys between 25 and 260°C and for the Al-4Li alloys at 25°C. Determinations of tensile properties were made on 3.18-mm diameter and 15.9-mm gage length subsize specimens according to ASTM E8-81. Compressive yield stresses of alloys in the T6 and T8 tempers were determined on cylindrical specimens 9.52 mm in diameter and 12.7 mm high. Most tensile and compressive properties data were based on triplicate or quadruplicate tests.

Fracture toughnesses of extrusions in the T8 temper were determined in the LT and TL orientations by use of subsize compact-tension specimens. Although the specimens were typically less than 1.27-cm thick, the measured toughness data were sufficiently low to be valid K_{IC} (plane-strain fracture toughness) values.

Fatigue-crack-growth-rate (FCGR) data for specimens in the T8 temper were determined in the LT and TL orientations by use of subsize compact-tension specimens. The test frequency was 5 Hz and the ratio of maximum to minimum load was 0.1.

Steady-state creep rates and stress-rupture data were determined for Al-3Cu-2Li-1Mg-1.6Cr-0.2Zr-T8 at 150°C by use of flat tensile specimens of 2.5-cm gage length. Tests were conducted under loads corresponding to 65, 75, and 85% of the 150°C yield stress of the alloy.

The general corrosion behavior of alloys in the T8 temper was determined from weight-loss measurements after 125 hr continuous immersion in an aqueous 3.5 wt% NaCl solution. The weight-loss data were converted to equivalent decreases in thickness for comparison with handbook data.

4. TASK 5: HIGH-STRENGTH RSP AL-3CU-2LI-1MG-0.2ZR ALLOYS FOR AMBIENT- AND ELEVATED-TEMPERATURE SERVICE

4.1 Evaluation of Dispersoid-Forming Additives

The compositions Al-1.8Cr, Al-3.9Y, Al-4.5Ce, and Al-6.5Er were chosen for investigation to yield approximately 5 vol% Al_7Cr , Al_3Y , Al_4Ce , or Al_3Er dispersoids, respectively. Typical microstructures of roller-quenched flakes are shown in Figure 2. Al-Cr flakes have a small volume fraction of discrete, 200- to 300-nm diameter dispersoids, with most of the Cr in metastable solid solution (Figure 2a). In contrast, the Al-Y, Al-Ce, and Al-Er flakes are microsegregated and typically have cellular microstructures (Figures 2b-2d). The average cell diameter is fixed by the solidification rate and is approximately the same for all three alloys. The as-quenched microstructures correspond qualitatively to the discussion of Section 2.2.1.

Samples of roller-quenched flakes were heat treated for 1 hr at 400, 500, 550, and 600°C to simulate the effect of consolidation processing on the development of dispersoid size and spacing. Transmission electron micrographs of heat-treated flakes reveal the process of dispersoid formation from the as-solidified microstructure (Figures 3-6).

In the Al-1.8Cr flakes, the metastable solid solution is preserved upon heat treatment at or below 500°C (compare Figures 2a, 3a, and 3b). Chromium-containing dispersoids precipitate between 500 and 550°C for a 1-hr heat treatment, and the dispersoids coarsen above 550°C. This sequence is favorable for control of mechanical properties because the temperature at which dispersoids form is above any temperature encountered in consolidation processing. The size and spacing of dispersoids can prospectively be controlled by appropriate post-consolidation heat treatments which simultaneously place Li, Cu, and Mg in solid solution. The dispersoid distribution is also independent of the alloy's solidification rate.

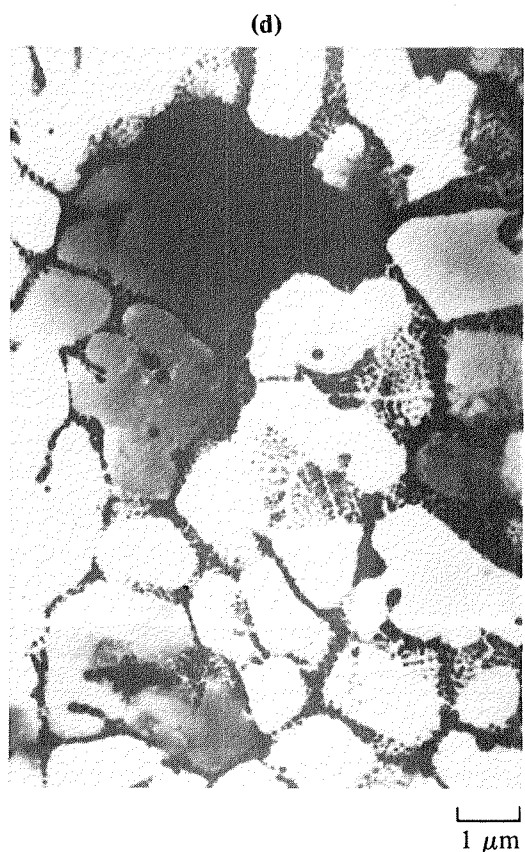
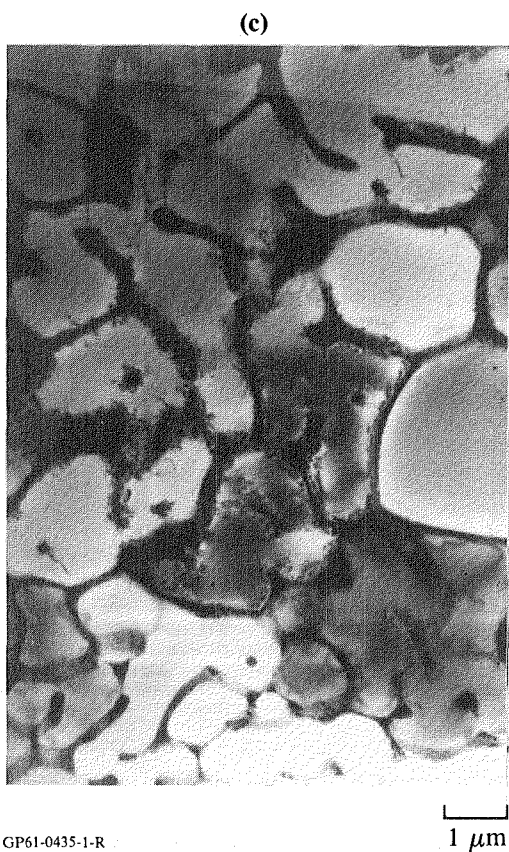
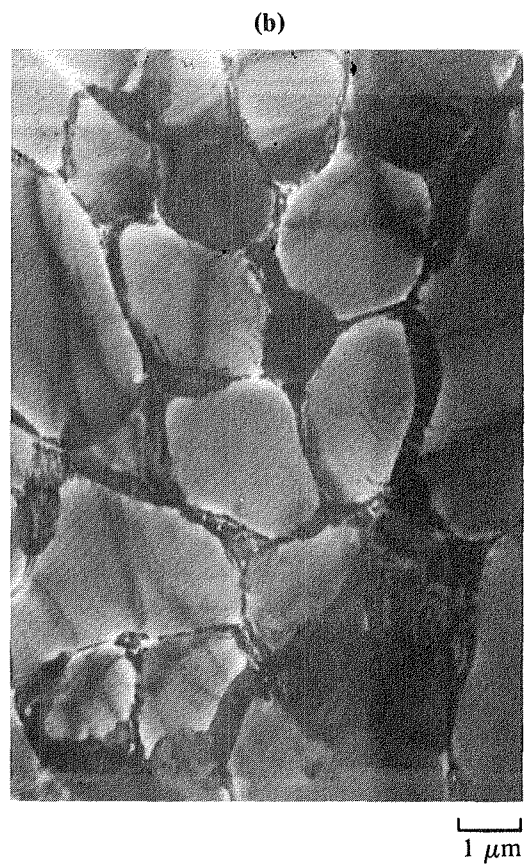
Dispersoids in rapidly solidified Al-Y, Al-Ce, and Al-Er alloys are formed by spheroidization of the as-solidified cellular microstructure (Figures 4-6). The optimal dispersoid size and spacing is generally attained after 500°C/1 hr heat treatment, implying significant coarsening after a typical solution treatment of 530°C/1 hr for dispersoid-containing Al-3Cu-2Li-1Mg-0.2Zr. Although system-to-system differences in dispersoid size and spacing do occur, with Al-6.5Er having the finest dispersoids after 500°C/1 hr heat treatment,

the distribution is controlled mainly by the original solidification rate. Indeed, apparent differences in dispersoid size (e.g., compare Figures 4a-4c or 4b, 5b, 6b) may result from flake-to-flake differences in solidification rate rather than from the specific systems involved.

Based on the fine dispersoid distribution and anticipated degree of microstructural control, 1.8Cr was chosen as the novel dispersoid-forming additive for the RSP Al-3Cu-2Li-1Mg-0.2Zr alloy. The conventional dispersoid-forming additive, 1Fe + 1Ni, was shown (1) to produce dispersoids similar in size, spacing, and formation kinetics to those in Figures 4-6. The following compositions were selected for Task 5 evaluation: Al-3Cu-2Li-1Mg-0.2Zr (baseline), Al-3Cu-2Li-1Mg-1Fe-1Ni-0.2Zr (conventional dispersoids), and Al-3Cu-2Li-1Mg-1.8Cr-0.2Zr (novel dispersoids).

4.2 Alloy Composition

Concentrations of major alloying elements in the three Al-3Cu-2Li-1Mg-0.2Zr alloys, determined at HMI by atomic absorption methods, are listed in Table 3. Analyzed concentrations are generally close to the nominal concentrations, and concentration differences of the same element from one alloy to the next are small, except that the Cr-containing alloy has 12-14% less Cu than the other two alloys. Total H and O concentrations (Table 3) are significantly smaller than those in previous RSP Al-Li extrusions produced from vacuum-atomized powder (1). The consolidation process for the present extrusions included a careful degassing cycle consisting of repeated washing of the green compact with argon while heating to the hot-pressing temperature. The vacuum hot-pressing step employed in the present consolidation sequence also may have improved degassing by expelling residual entrained gases prior to extrusion.



GP61-0435-1-R

Figure 2. Transmission electron micrographs of roller-quenched flakes: (a) Al-1.8Cr, (b) Al-3.9Y, (c) Al-4.5Ce, and (d) Al-6.5Er.

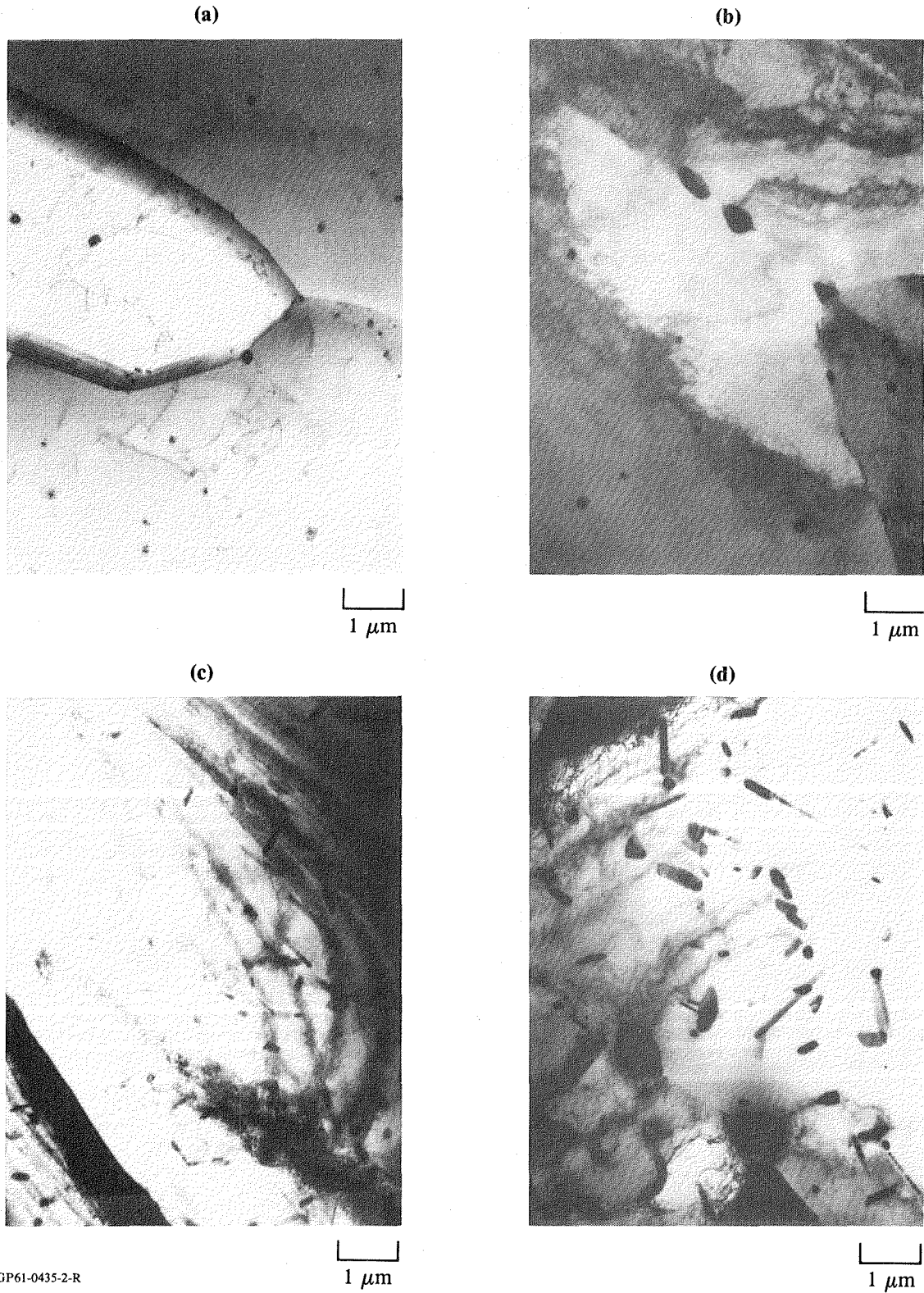
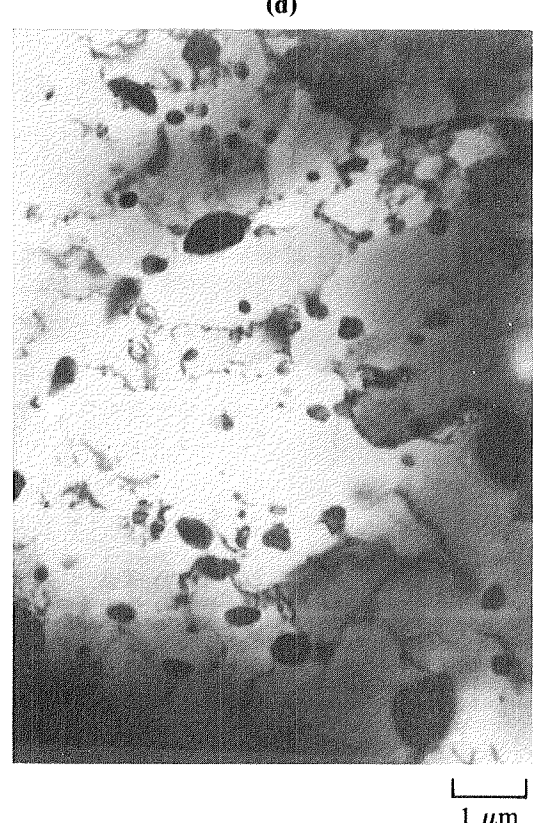
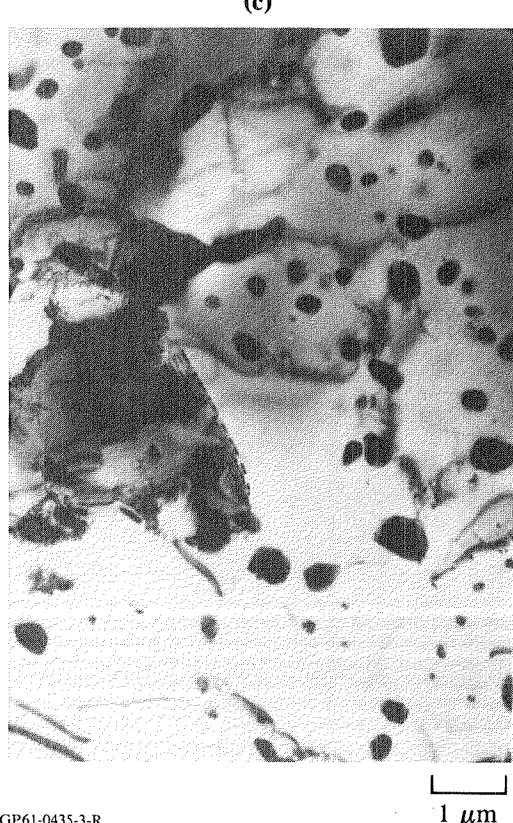
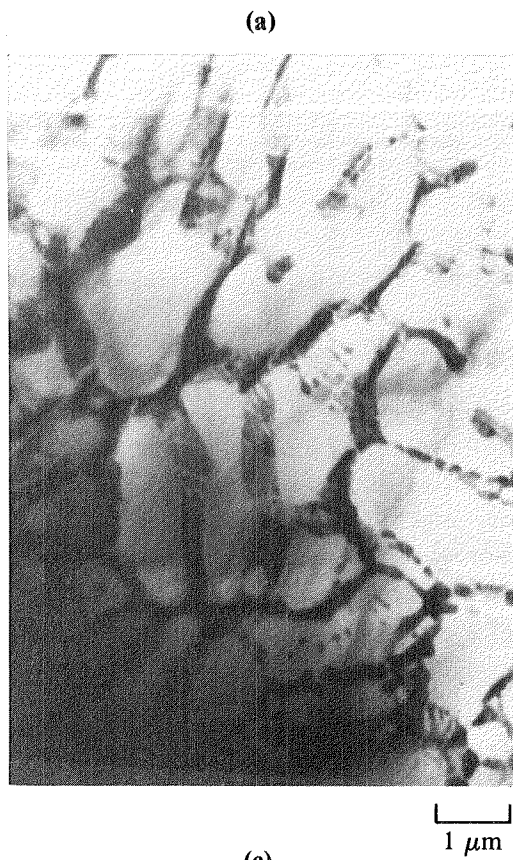


Figure 3. Transmission electron micrographs of roller-quenched Al-1.8Cr flakes heat treated for 1 hr at (a) 400, (b) 500, (c) 550, and (d) 600°C.



GP61-0435-3-R

Figure 4. Transmission electron micrographs of roller-quenched Al-3.9Y flakes heat treated for 1 hr at (a) 400°C, (b) 500°C, (c) 550°C, and (d) 600°C.

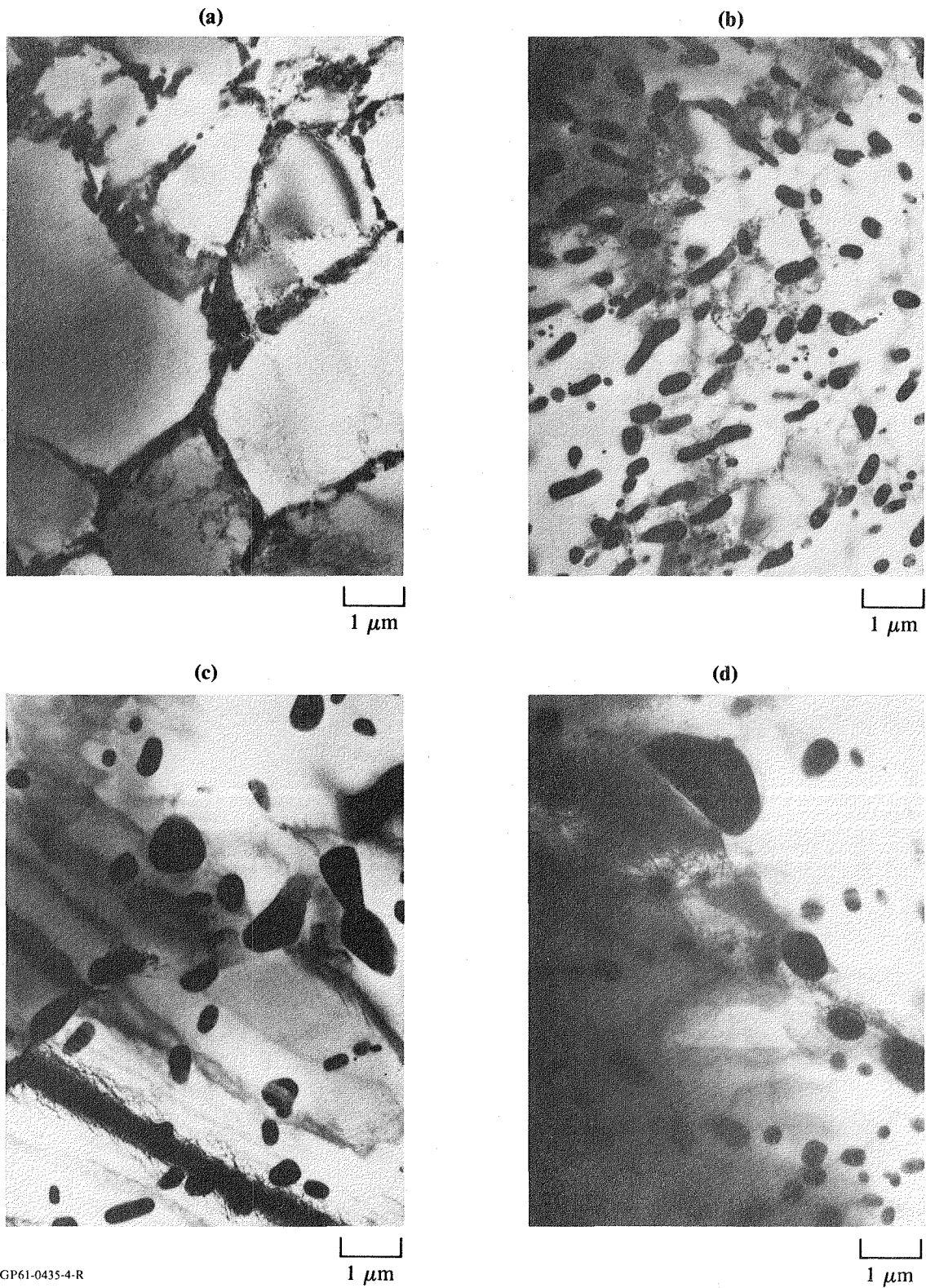
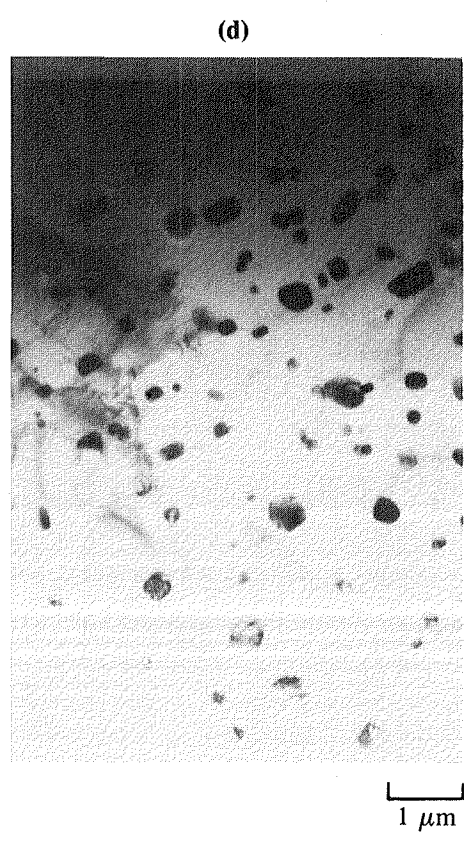
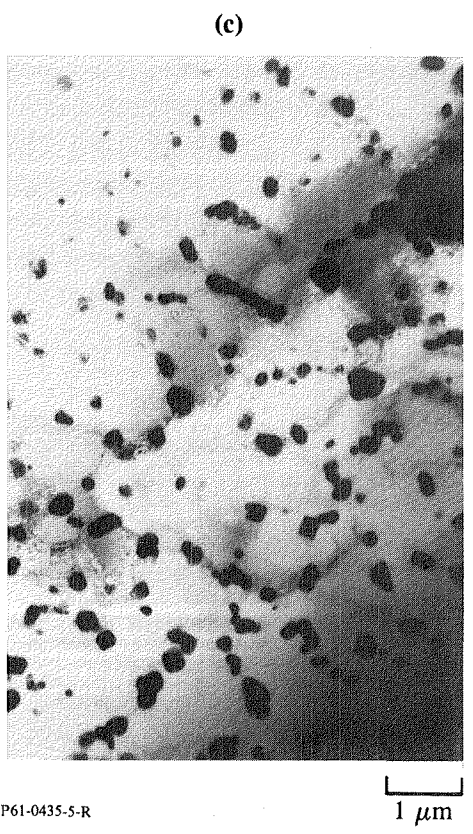
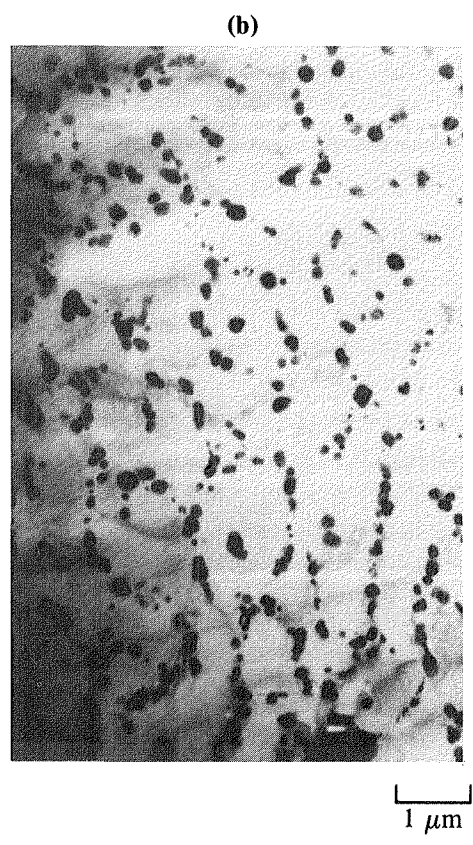
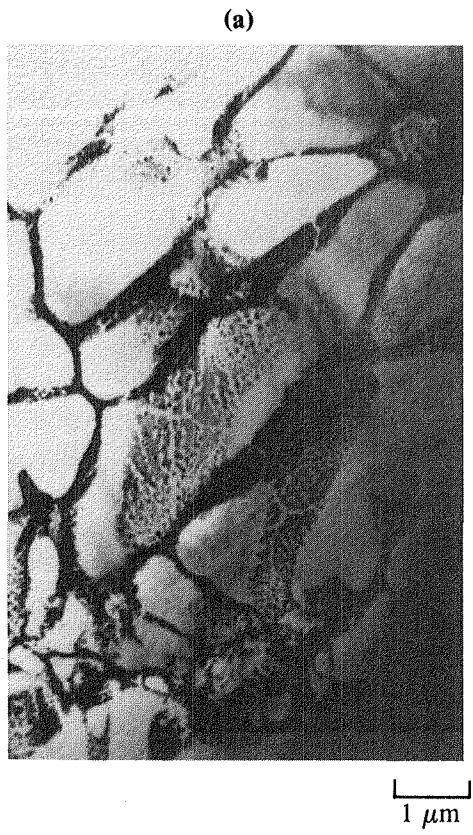


Figure 5. Transmission electron micrographs of roller-quenched Al-4.5Ce flakes heat treated for 1 hr at (a) 400°C, (b) 500°C, (c) 550°C, and (d) 600°C.



GP61-0435-5-R

Figure 6. Transmission electron micrographs of roller-quenched Al-6.5Er flakes heat treated for 1 hr at (a) 400°C, (b) 500°C, (c) 550°C, and (d) 600°C.

TABLE 3. COMPOSITIONS OF RSP Al-3Cu-2Li-1Mg-0.2Zr ALLOYS.

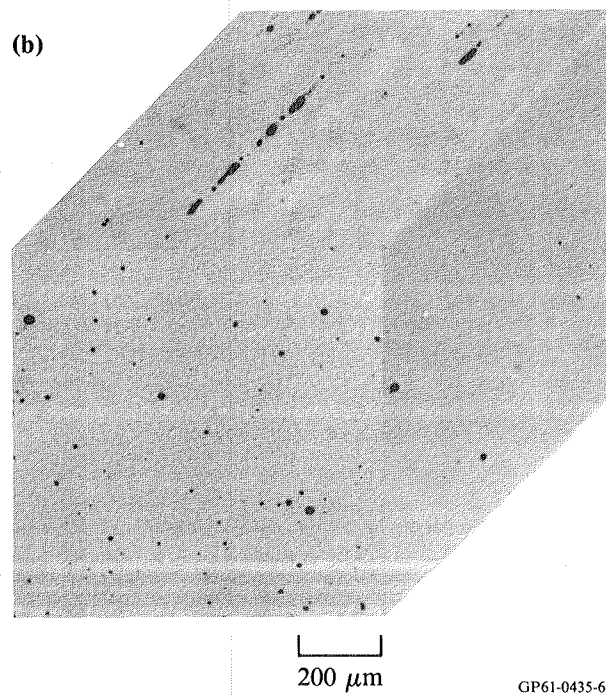
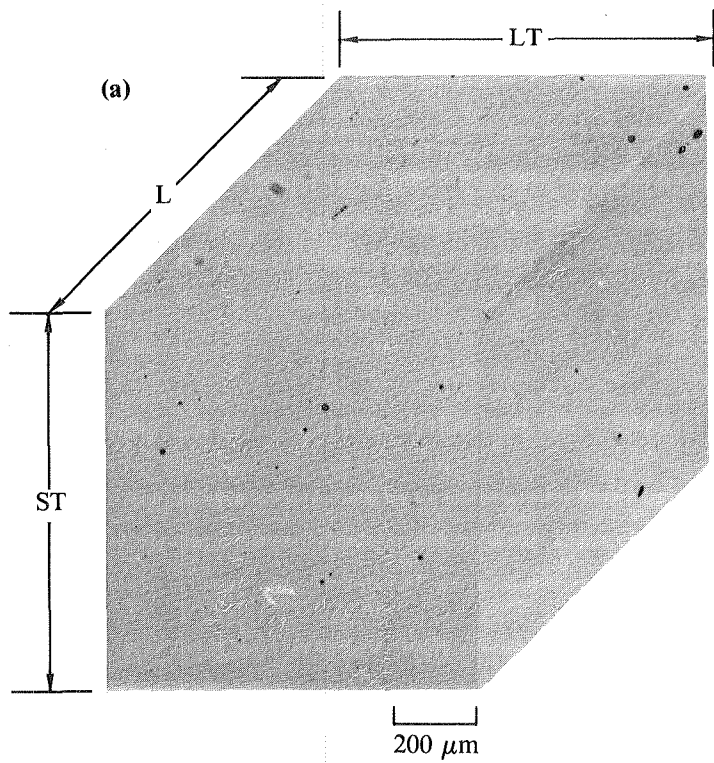
Nominal composition	Analyzed composition						
	Weight %					Weight ppm	
	Cu	Li	Mg	Zr	Fe, Ni, Cr	O	H
Al-3Cu-2Li-1Mg-0.2Zr	3.19	2.0	1.07	0.22	—	190 ±70	1.6
Al-3Cu-2Li-1Mg-1Fe-1Ni-0.2Zr	3.12	2.0	0.94	0.21	1.0 Fe + 0.96 Ni	250 ±100	1.6
Al-3Cu-2Li-1Mg-1.8Cr-0.2Zr	2.75	2.1	1.04	0.22	1.64 Cr	340 ±110	2.8
Al-3Li-1.5Cu-1Mg-0.5Co-0.2Zr (extrusion from vacuum- atomized powder, Ref. 1)	—	—	—	—	—	480 ±60	<20

GP61-0435-31-R

4.3 Microstructure

4.3.1 Evaluation of Inclusions

RSP aluminum alloy powders often have inclusions, which may be foreign particles (e.g., Ni- or Fe-base alloys owing to cross-contamination) or oxide particles formed in the melt or by subsequent interaction of the particulates with oxygen, water vapor, or carbon dioxide. Polished but unetched sections of solution-treated Al-3Cu-2Li-1Mg-0.2Zr extrusions were examined to characterize the size and distribution of such inclusions (Figure 7). Approximately 0.3 vol% of 2- to 30- μ m diameter inclusions was observed in the baseline Al-3Cu-2Li-1Mg-0.2Zr alloy and approximately 0.6 vol% in the Al-3Cu-2Li-1Mg-1Fe-1Ni-0.2Zr alloy. The inclusions tend to appear as stringers, particularly in the [Fe + Ni]-containing alloy. The inclusions were not characterized in detail, but similar inclusions in RSP Al-4Li alloys (10) were identified as aluminum or aluminum-lithium oxides by energy-dispersive x-ray analysis. The oxides were thought to have originated in the melt by interaction of Al and Li with furnace-lining refractories, the argon atmosphere (which contains parts-per-million oxygen concentrations), or both. No evidence of cross-contaminant particles has been found in vacuum-atomized Al alloy powders produced recently by HMI for MDRL. The observed inclusions are expected to degrade transverse tensile properties and fracture toughnesses of the RSP alloys.



GP61-0435-6-R

Figure 7. Optical photomicrographs of unetched samples of (a) Al-3Cu-2Li-1Mg-0.2Zr and (b) Al-3Cu-2Li-1Mg-1Fe-1Ni-0.2Zr extrusions, solution-treated 560°C/1 h.

4.3.2 As-Extruded Condition

Optical photomicrographs of Al-3Cu-2Li-1Mg-0.2Zr alloys in the as-extruded condition are shown in Figure 8. The dark, 1- to 10- μ m-diameter constituent particles are predominantly T_2 (Al_5Li_3Cu) according to the 400°C isothermal section of the Al-Li-Cu phase diagram (20), although the phase S (Al_2CuMg) may also be present (20,21). Lightly etched, 1- to 2-mm-diameter particles may be Al_2LiMg , oxides resulting from disintegration of oxide skins on the original particulates during extrusion, or [Fe + Ni]- or Cr-containing dispersoids (in Figures 8b and 8c). Constituent and dispersed phases not containing copper are virtually indistinguishable in polished and etched samples, and x-ray diffractometry is required to identify such phases unambiguously. The lack of an observable grain structure is typical of the fully-recovered, unrecrystallized substructures which are stabilized by the coherent Al_3Zr dispersoids that normally appear in Zr-containing RSP Al-Li alloys. The microstructures are uniform throughout the extrusions and reflect the uniformity of the RSP particulates.

Phases identified in x-ray diffraction patterns of as-extruded Al-3Cu-2Li-1Mg-0.2Zr alloys are summarized in Table 4. The copper-containing constituent phase in Figure 8a (and by extension those in Figures 8b and 8c) is largely T_2 . The dispersed phase in Al-3Cu-2Li-1Mg-1Fe-1Ni-0.2Zr is Al_9FeNi as predicted from the Al-Fe-Ni equilibrium phase diagram (20). The 400°C isothermal section of the Al-Cr-Mg phase diagram (20) shows the composition 1Mg,

**TABLE 4. CONSTITUENT AND DISPERSED PHASES
IN AS-EXTRUDED AND SOLUTION-TREATED
Al-3Cu-2Li-1Mg-0.2Zr ALLOYS.**

Alloy composition	Phases present in indicated condition	
	As-extruded	Solution-treated 560°C/1 h
Al-3Cu-2Li-1Mg-0.2Zr	T_2 (Al_5Li_3Cu), others	Peak intensities too small for identification
Al-3Cu-2Li-1Mg-1Fe-1Ni-0.2Zr	Al_9FeNi , others	Al_9FeNi , others
Al-3Cu-2Li-1Mg-1.6Cr-0.2Zr	$Al_{18}Cr_2Mg_3$, others	$Al_{18}Cr_2Mg_3$

GP61-0435-32-R

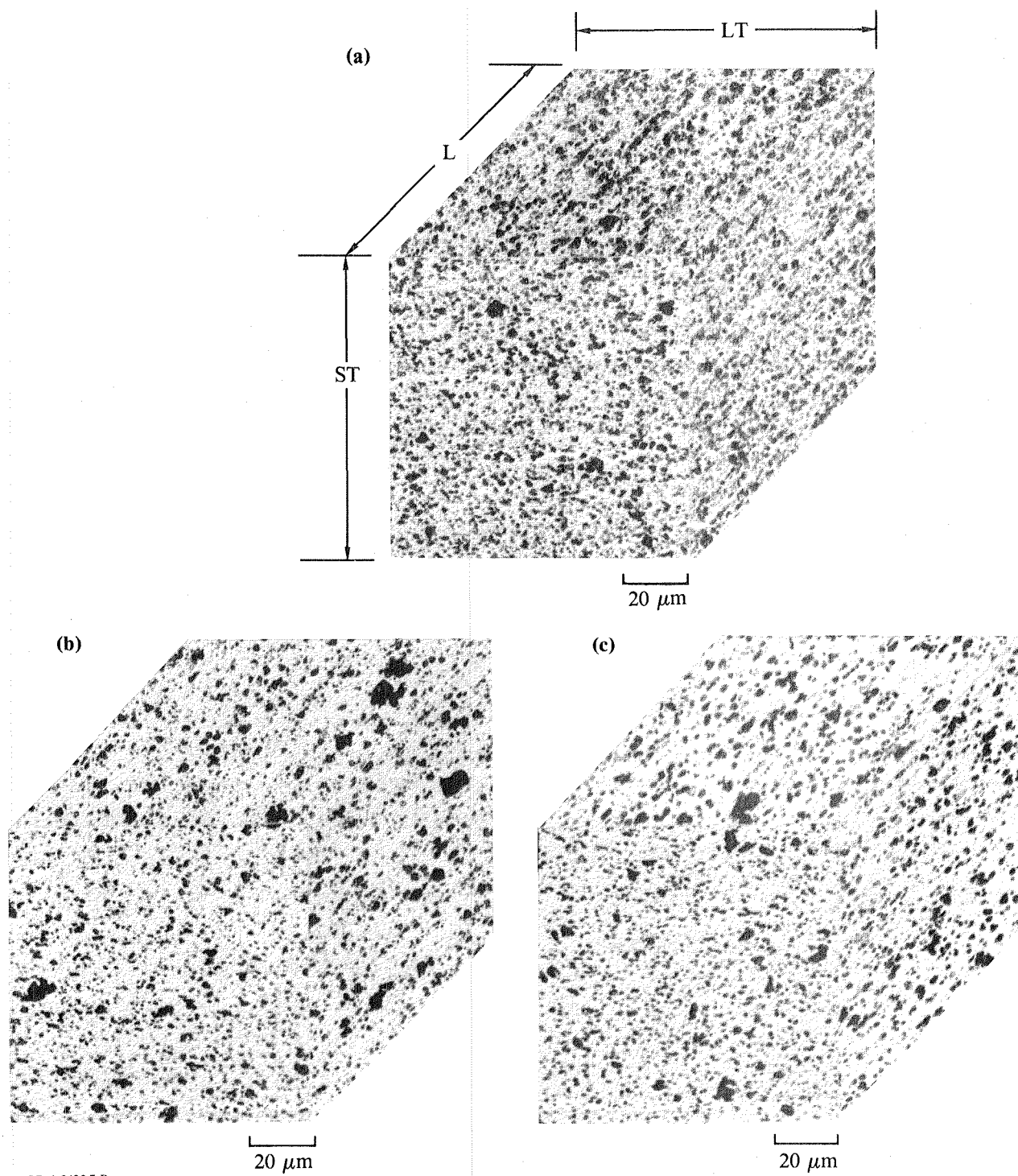


Figure 8. Optical photomicrographs of as-received extrusions of (a) Al-3Cu-2Li-1Mg-0.2Zr, (b) Al-3Cu-2Li-1Mg-1Fe-1Ni-0.2Zr, and (c) Al-3Cu-2Li-1Mg-1.6Cr-0.2Zr.

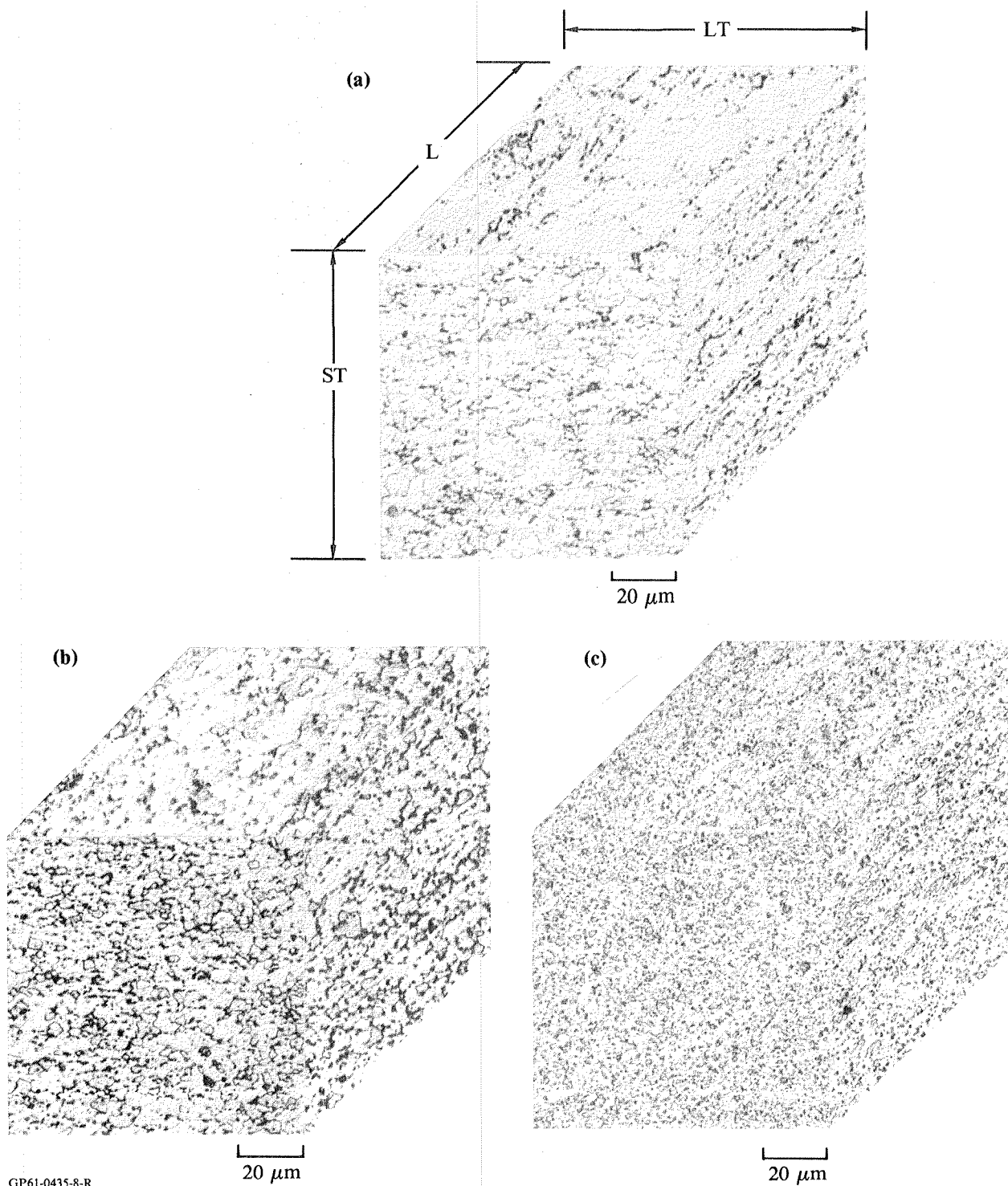
1.6Cr as being in the three-phase (Al) + Al₇Cr + Al₁₈Cr₂Mg₃ field, but only the latter phase is found by x-ray diffraction. The diffraction patterns show numerous weak lines which correspond to the other constituent and dispersed phases mentioned above.

4.3.3 Solution-Treated Condition

Optical photomicrographs of Al-3Cu-2Li-1Mg-0.2Zr alloys, solution-treated for 1 hr at 560°C, are shown in Figure 9. Solution-treatment takes almost all of the Li, Cu, and Mg into solid solution, leaving a small volume fraction of 1- to 2- μ m-diameter constituent particles (Figure 9a). Crooks and Starke (21) have identified similar particles in an RSP Al-3Cu-1.6Li-0.8Mg-0.2Zr alloy as being predominantly T₂ at grain boundary triple points, with some S phase present on grain boundaries. Homogeneous distributions of dispersed phases are observed in Figures 9b and 9c. Some high-angle grain boundaries are visible, particularly in Figure 9b. These boundaries result from partial polygonization of the as-extruded mosaic substructure by boundary rearrangement during solution treatment (10). The solution-treated grain structure is a mixture of high- and low-angle boundaries. Since nucleation of new grains does not take place and the crystallographic texture is virtually unaltered, the microstructure is still regarded as unrecrystallized (10).

Dispersoid and grain/subgrain sizes can be evaluated from transmission electron micrographs of solution-treated samples (Figure 10). Geometric mean subgrain diameters of the three alloys are: Al-3Cu-2Li-1Mg-0.2Zr, 3.7 μ m; Al-3Cu-2Li-1Mg-1Fe-1Ni-0.2Zr, 4.0 μ m; and Al-3Cu-2Li-1Mg-1.6Cr-0.2Zr, 2.1 μ m. Both [Fe + Ni]- and Cr-containing alloys have incoherent dispersoids ranging in diameter from ~ 0.4 to ~ 2 μ m, with a mean diameter of approximately 1 μ m (Figures 10b and 10c). In addition, the Cr-containing alloy has numerous equiaxed or rod-shaped, 0.15- to 0.3- μ m-diameter dispersoids which are similar in size to Al₁₈Cr₂Mg₃ dispersoids found in 7075-Al (22). In an alloy without Zr such dispersoids exert a grain-refining effect, but it is doubtful whether they can be the cause of subgrain refinement in the present alloys because of the more powerful effect of coherent Al₃Zr dispersoids.

X-ray diffraction patterns of solution-treated samples do not yield any lines from constituent phases, owing to their small volume fractions (Table 4). Retention of the phase Al₁₈Cr₂Mg₃ after solution treatment is not inferred from the Al-Cr-Mg equilibrium diagram, which predicts that Al₇Cr



GP61-0435-8-R

Figure 9. Optical photomicrographs of (a) Al-3Cu-2Li-1Mg-0.2Zr, (b) Al-3Cu-2Li-1Mg-1Fe-1Ni-0.2Zr, and (c) Al-3Cu-1Li-1Mg-1.6Cr-0.2Zr extrusions, solution-treated at 560°C for 1 hr.

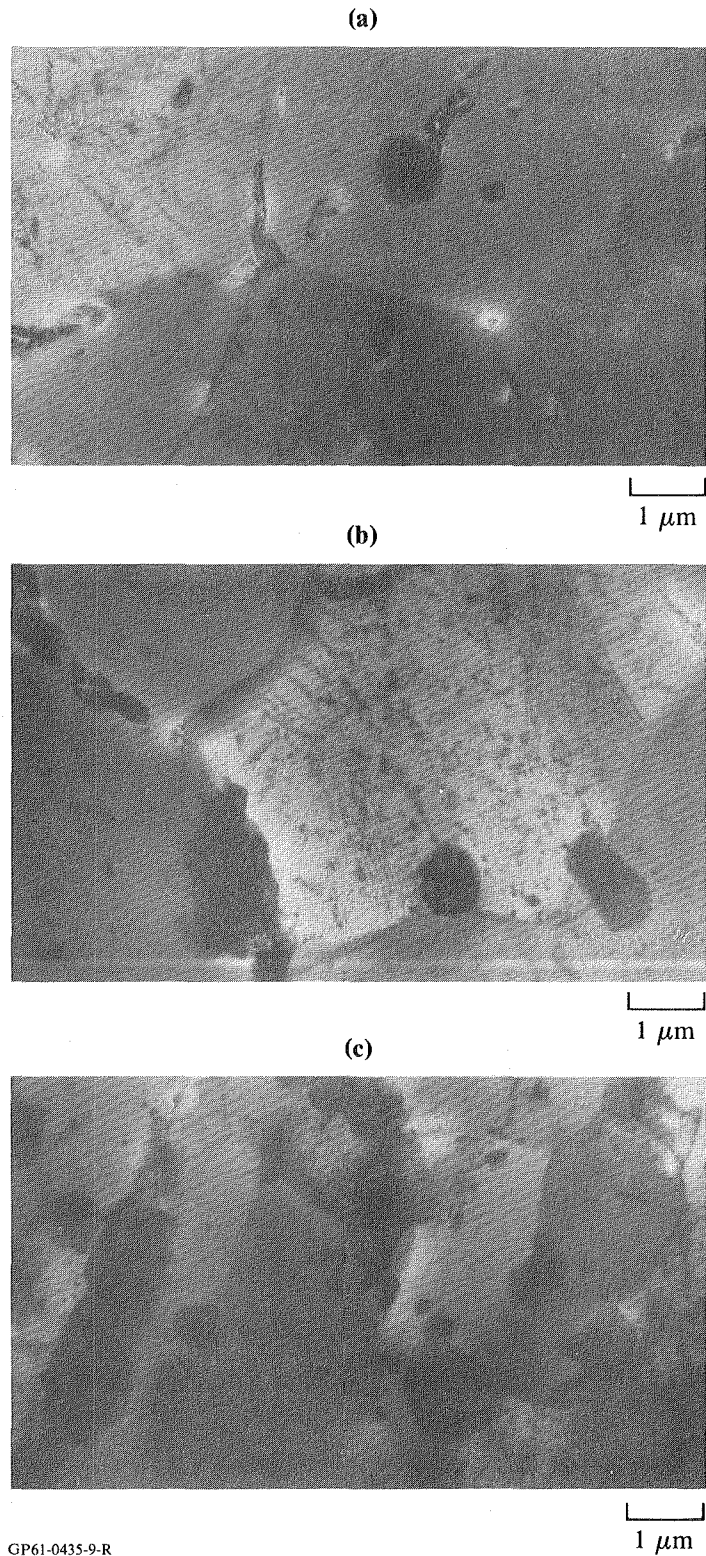


Figure 10. Transmission electron photomicrographs of 560°C solution-treated and quenched (a) Al-3Cu-2Li-1Mg-0.2Zr, (b) Al-3Cu-2Li-1Mg-1Fe-1Ni-0.2Zr, and (c) Al-3Cu-2Li-1Mg-1.6Cr-0.2Zr.

should form upon 560°C solution treatment. Reduction in solubility of Mg in the matrix by the multicomponent Cu and Li additions may make more Mg available for dispersoid formation than in a ternary alloy, favoring the formation of the Mg-rich dispersed phase.

4.3.4 Aged Conditions

Crooks and Starke (21) have identified the major precipitate phases in peak-aged RSP Al-3Cu-1.6Li-0.8Mg-0.2Zr as T_1 (Al_2CuLi), S' (Al_2CuMg), and their precursors. Both phases are plate-like and tend to nucleate on matrix dislocations and favorably oriented low-angle boundaries. In the T6 condition (solution-treated and peak-aged), the precipitates are relatively coarse and widely spaced, whereas in the T8 condition (solution-treated, stretched, and peak-aged) the density of nucleation sites for T_1 and S' is increased considerably, resulting in a much larger concentration of finer plate-like precipitates. Homogeneous precipitate nucleation in the T8 condition virtually eliminates the grain-boundary precipitate-free zone (PFZ) which is found in the T6 condition and in Al-Li and Al-Cu-Li alloys strengthened primarily by the phase δ' (Al_3Li). This phase was not observed in the Al-3Cu-1.6Li-0.8Mg-0.2Zr alloy in any temper (21).

Transmission electron photomicrographs of the Al-3Cu-2Li-1Mg-0.2Zr alloys (Figures 11-13) generally show the features identified by Crooks and Starke (21). Grain boundaries (Figures 11c and 11d) and incoherent dispersoids (Figures 12d and 13d) do not have PFZs. The phase δ' appears in all three alloys in the T6 condition (Figures 11b, 12b, and 13b), and dark-field TEM photomicrographs show that small amounts of δ' are present in all three alloys in the T8 condition as well. The phase δ' appears in these alloys because they have larger Li concentrations than in the alloy investigated by Crooks and Starke (21). The larger T_1 and S' concentrations in the T8 condition as compared with the T6 condition are expected to result in higher yield stresses for alloys in the T8 temper.

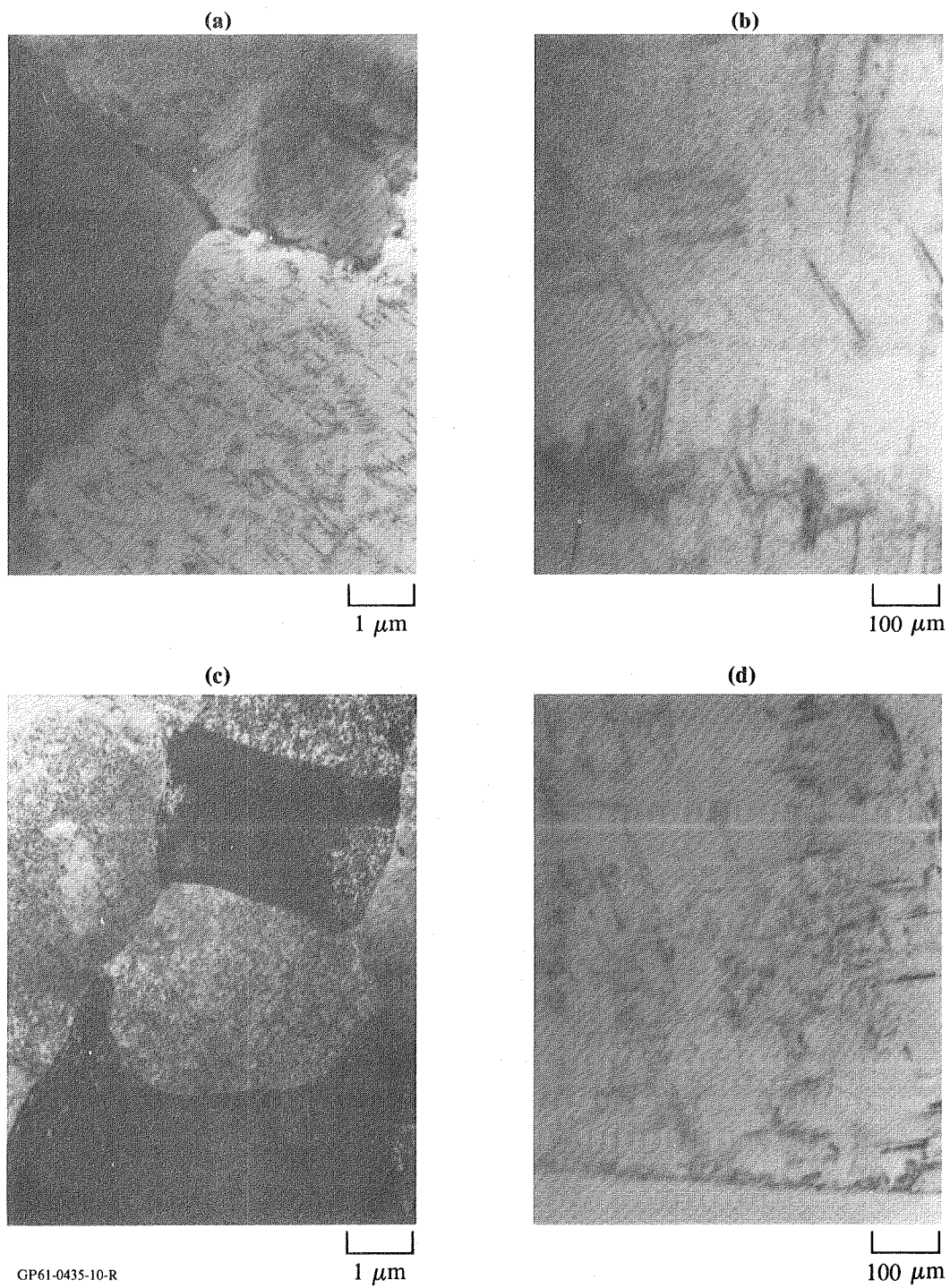
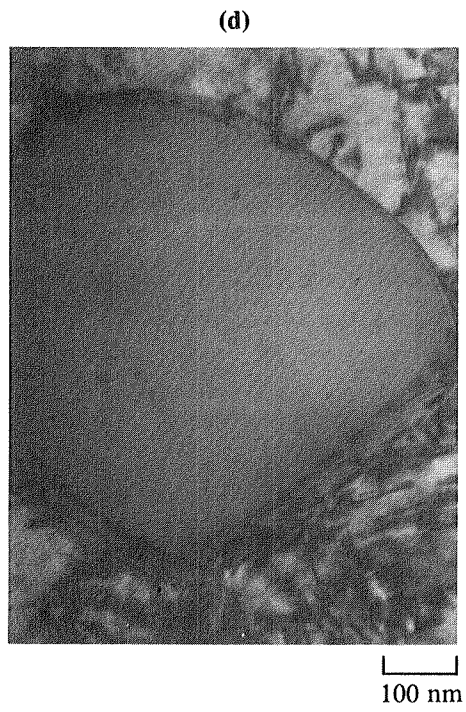
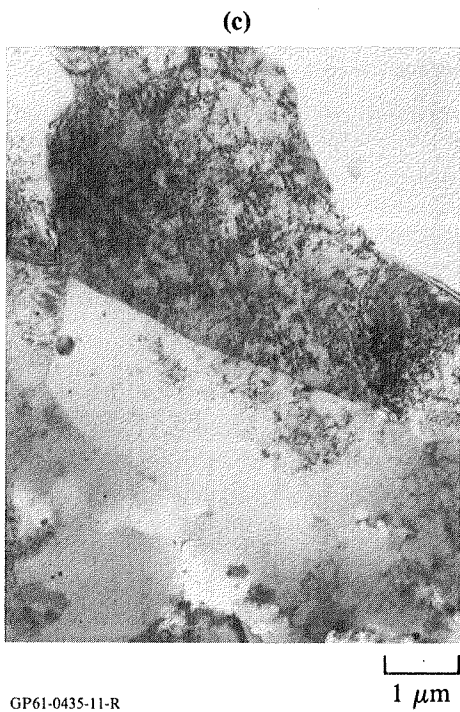
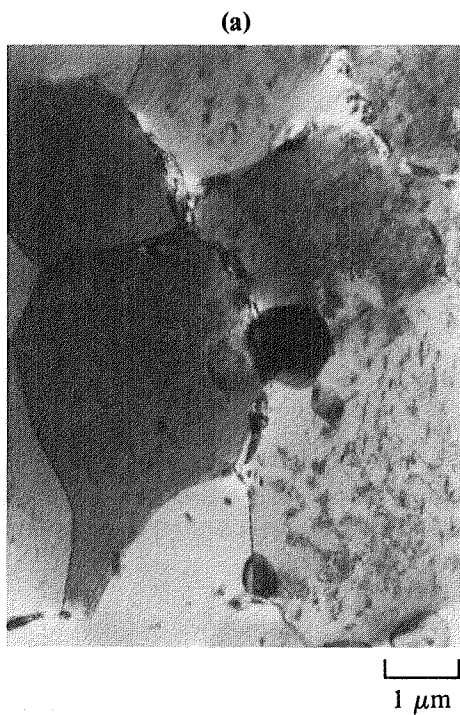


Figure 11. Transmission electron photomicrographs of 560°C solution-treated and aged RSP Al-3Cu-2Li-1Mg-0.2Zr; (a), (b) T6 temper, and (c), (d) T8 temper.



GP61-0435-11-R

Figure 12. Transmission electron photomicrographs of 560°C solution-treated and aged RSP Al-3Cu-2Li-1Mg-1Fe-1Ni-0.2Zr; (a), (b) T6 temper, and (c), (d) T8 temper.

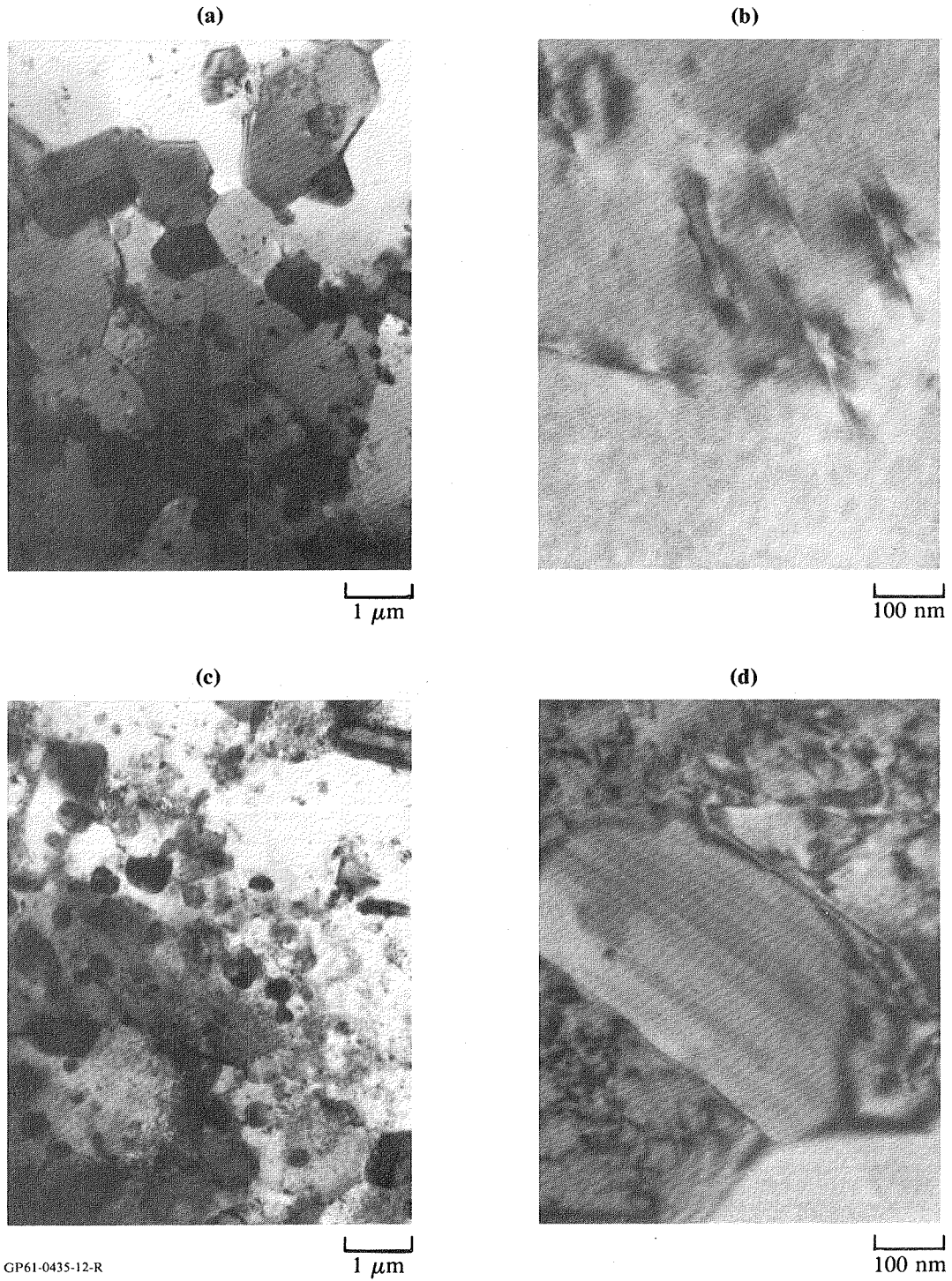


Figure 13. Transmission electron photomicrographs of 560°C solution-treated and aged Al-3Cu-2Li-1Mg-1.6Cr-0.2Zr; (a), (b) T6 temper, and (c), (d) T8 temper.

4.4 Properties

4.4.1 Density and Elastic Modulus

Densities and elastic moduli of the Al-3Cu-2Li-1Mg-0.2Zr alloys are listed in Table 5. The data are comparable to those for Al-2.9Cu-2.2Li-1.0Mg-0.2Zr reported by Palmer et al. (17). The modulus/density ratios are approximately 20% larger than for commercial 2XXX and 7XXX aluminum alloys.

4.4.2 Mechanical Properties

Ambient-temperature tensile properties of the Al-3Cu-2Li-1Mg-0.2Zr alloys in the T6 and T8 tempers are listed in Table 6. The strength of RSP Al-3Cu-2Li-1Mg-0.2Zr-T6 is equal to that of a similar alloy examined by Palmer et al. (17) and is slightly larger than that of an alloy lower in Li examined by Crooks and Starke (21). The strength of the Al-3Cu-2Li-1Mg-0.2Zr alloy in the T8 temper appears to be too high, both in relation to other data and relative to the data for the dispersoid-containing alloys, which are stronger than the baseline alloy in the T6 condition. The T8 compressive yield stress of this alloy is 577 MPa, which agrees well with other determinations. Ductilities of the present alloys are similar to those of the powder-source alloy examined by Palmer et al. (17), and are slightly lower than those of the splat-source alloy investigated by Crooks and Starke (21), perhaps owing to lower inclusion and oxide concentrations in the latter material.

Long-transverse (LT) yield stresses (Table 7) are typically 91-98% of the longitudinal (L) yield stresses, while LT ultimate tensile stresses are typically 85-93% as large as L ultimate tensile stresses. The LT/L strength ratios are somewhat better for specimens in the T8 temper than in the T6 temper. LT specimens typically have 2% lower elongations than L specimens. These results are comparable to those obtained for RSP Al-3Li alloys at this strength level (8), and are considered to reflect good powder consolidation practice.

The effect of changing heat treatment variables on strength/ductility relationships was explored by determining tensile properties of specimens in the T3 (560°C/1 hr + 2% stretch + 25°C/168 hr)(naturally aged) and underaged T8 (560°C/1 hr + 2% stretch + 160°C/16 hr) tempers (Table 8). Adding Al₉FeNi dispersoids to the baseline composition increases the T3 yield stress by 28 MPa, an increase similar to the 33 MPa observed for the T6 temper. Use of

TABLE 5. MASS DENSITIES AND ELASTIC MODULI OF Al-3Cu-2Li-1Mg-0.2Zr ALLOYS.

Alloy composition	Mass density (g/cm ³)	% reduction relative to 7075-Al	Elastic modulus (GPa)	Modulus/density ratio (GPa cm ³ g ⁻¹)
Al-3Cu-2Li-1Mg-0.2Zr	2.590	7.5	79.2 ± 4.0	30.6
Al-3Cu-2Li-1Mg-1Fe-1Ni-0.2Zr	2.620	6.4	80.5 ± 3.0	30.7
Al-3Cu-2Li-1Mg-1.6Cr-0.2Zr	2.586	7.6	77.0 ± 2.1	29.8
Al-2.9Cu-2.2Li-1.0Mg-0.21Zr (Ref. 17)	2.58	7.9	78.3	30.3
2124-Al	2.77	—	71	25.6
7075-Al	2.80	—	72	25.7

GP61-0435-33-R

TABLE 6. AMBIENT-TEMPERATURE LONGITUDINAL MECHANICAL PROPERTIES OF PEAK-AGED Al-3Cu-2Li-1Mg-0.2Zr ALLOYS.

Alloy composition	Temper	Yield stress (MPa [ksi])	Ultimate tensile stress (MPa [ksi])	Elongation (%)
Al-3Cu-2Li-1Mg-0.2Zr	T6	508 ± 44 (73.7 ± 6.4)	601 ± 34 (87.2 ± 4.9)	5.3 ± 1.8
	T8	627 ± 35 (90.9 ± 5.0)	662 ± 24 (96.1 ± 3.5)	6.4 ± 1.9
Al-3Cu-2Li-1Mg-1Fe-1Ni-0.2Zr	T6	541 ± 46 (78.4 ± 6.6)	622 ± 27 (90.3 ± 3.9)	3.7 ± 0.8
	T8	588 ± 19 (85.3 ± 2.8)	624 ± 13 (90.4 ± 2.0)	4.2 ± 0.5
Al-3Cu-2Li-1Mg-1.6Cr-0.2Zr	T6	552 ± 35 (80.1 ± 5.1)	628 ± 19 (91.1 ± 2.8)	4.4 ± 1.4
	T8	605 ± 16 (87.7 ± 2.3)	644 ± 7 (93.4 ± 1.1)	4.3 ± 0.7
Al-2.9Cu-2.2Li-1.0Mg-0.21Zr (Ref. 17)	T6	497 (72.1)	592 (85.9)	7.1
	T8	578 (83.8)	604 (87.6)	5.3
Al-3.0Cu-1.6Li-0.8Mg-0.2Zr (Ref. 21)	T6	475 (68.9)	—	6.5
	T8	555 (80.5)	—	8.8
7075 (Ref. 16)	T651	503 (73)	573 (83)	11
	T7651	462 (67)	524 (76)	11

GP61-0435-34-R

TABLE 7. AMBIENT-TEMPERATURE LONG-TRANSVERSE MECHANICAL PROPERTIES OF Al-3Cu-2Li-1Mg-0.2Zr ALLOYS.

Alloy composition	Temper	Yield stress (MPa [ksi])	Ultimate tensile stress (MPa [ksi])	Elongation (%)
Al-3Cu-2Li-1Mg-0.2Zr	T6	481 ± 2 (69.8 ± 0.3)	533 ± 16 (77.3 ± 2.3)	3.1 ± 0.8
	T8	586 ± 11 (85.0 ± 1.6)	616 ± 14 (89.3 ± 2.0)	4.4 ± 0.8
Al-3Cu-2Li-1Mg-1Fe-1Ni-0.2Zr	T6	491 ± 4 (71.2 ± 0.6)	529 ± 13 (76.8 ± 1.9)	2.3 ± 0.4
	T8	579 ± 7 (84.0 ± 1.0)	597 ± 6 (86.6 ± 0.9)	2.1 ± 0.2
Al-3Cu-2Li-1Mg-1.6Cr-0.2Zr	T6	505 ± 2 (73.3 ± 0.2)	558 ± 5 (81.0 ± 0.8)	2.7 ± 0.2
	T8	573 ± 11 (83.1 ± 1.6)	585 ± 15 (84.9 ± 2.2)	2.4 ± 0.5

GP61-0435-35-R

TABLE 8. LONGITUDINAL MECHANICAL PROPERTIES OF Al-3Cu-2Li-1Mg-0.2Zr ALLOYS IN THE – T3 AND UNDERAGED – T8 TEMPER

Alloy composition	Temper	Yield stress (MPa [ksi])	Ultimate tensile stress (MPa [ksi])	Elongation (%)
Al-3Cu-2Li-1Mg-0.2Zr	T3	417 ± 18 (60.4 ± 2.6)	500 ± 9 (72.5 ± 1.3)	6.8 ± 1.1
	T8U	490 ± 8 (71.1 ± 1.1)	571 ± 3 (82.8 ± 0.4)	7.2 ± 0.9
Al-3Cu-2Li-1Mg-1Fe-1Ni-0.2Zr	T3	445 ± 24 (64.5 ± 3.4)	515 ± 21 (74.6 ± 3.0)	5.6 ± 1.1
	T8U	578 ± 12 (83.9 ± 1.7)	622 ± 10 (90.2 ± 1.4)	4.4 ± 0.1
Al-3Cu-2Li-1Mg-1.6Cr-0.2Zr	T3	362 ± 18 (52.6 ± 2.6)	430 ± 6 (62.4 ± 0.9)	7.2 ± 1.8
	T8U	509 ± 19 (73.8 ± 2.8)	569 ± 14 (82.5 ± 2.0)	4.3 ± 0.8
2024-Al (Ref. 16)	T351	325 (47.1)	470 (68.2)	20
Al-3Cu-2Li-1Mg-0.2Zr (Ref. 17)	T3	387 (56.2)	483 (70.0)	7.6

GP63-0435-36-R

natural rather than artificial aging does not significantly improve the ductilities of these alloys (compare Table 8 with Table 6), a conclusion also reached by Palmer *et al.* (17). Similarly, underaging in the T8 temper reduces the yield stress by 80-100 MPa in the baseline and Cr-containing alloys without improving ductility, while the strength and ductility of the [Fe + Ni]-containing alloy are unaffected by underaging.

Compressive yield stresses (Table 9) are equal to tensile yield stresses of the corresponding alloys and tempers except for Al-3Cu-2Li-1Mg-0.2Zr in the T8 temper; the measured tensile yield stress of this latter alloy is believed to be anomalously high. The compression data may yield a more accurate measure of the yield stress than the tensile data, particularly in the T6 temper, because of the larger cross-section and lowered susceptibility to machining stresses in the compression specimens. Compressive and tensile yield stresses in these alloys may be taken as equal for design purposes.

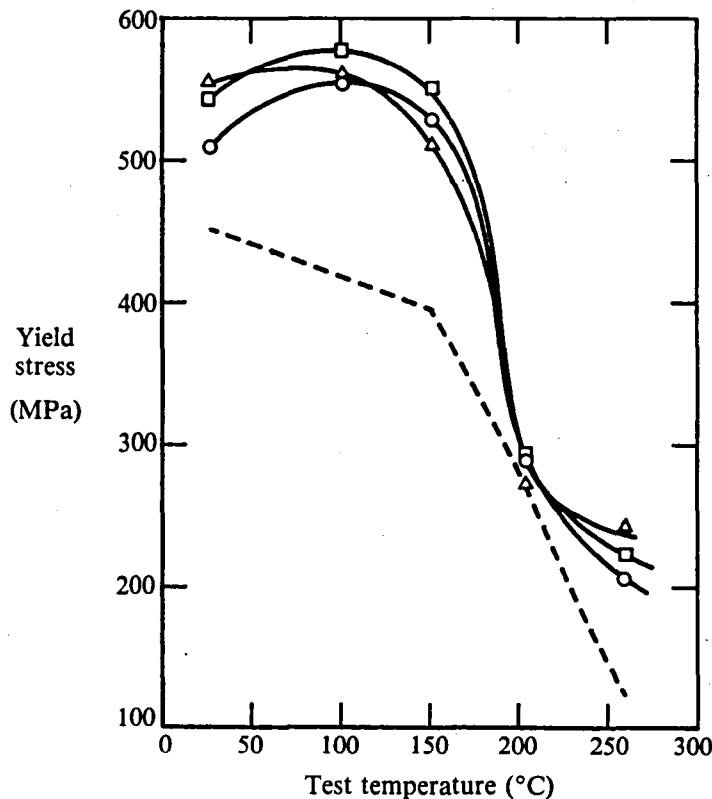
Elevated-temperature tensile properties of RSP Al-3Cu-2Li-1Mg-0.2Zr alloys are summarized in Figures 14-21. Increasing the test temperature from 25 to 150°C generally causes little change in yield stresses in the T6 (Figure 14) and T8 (Figure 17) tempers. In contrast, the yield stress of 2124-T851 decreases about 10% between 25 and 150°C (16). The T8-temper yield stresses of the RSP alloys are larger than those of 2124-T851 by approximately 35% at 25°C and 45% at 150°C. Similarly, the T6 (Figure 15) and T8 (Figure 18)

TABLE 9. AMBIENT-TEMPERATURE COMPRESSIVE YIELD STRESSES OF Al-3Cu-2Li-1Mg-0.2Zr ALLOYS.

Alloy composition	Temper	Compressive yield stress (MPa [ksi])	Tensile yield stress (MPa [ksi])
Al-3Cu-2Li-1Mg-0.2Zr	T6	501 ± 8 (72.7 ± 1.2)	508 ± 44 (73.7 ± 6.4)
	T8	577 ± 8 (83.6 ± 1.1)	627 ± 35 (90.9 ± 5.0)
Al-3Cu-2Li-1Mg-1Fe-1Ni-0.2Zr	T6	519 ± 10 (75.3 ± 1.4)	541 ± 46 (78.4 ± 6.6)
	T8	584 ± 12 (84.7 ± 1.8)	588 ± 19 (85.3 ± 2.8)
Al-3Cu-2Li-1Mg-1.6Cr-0.2Zr	T6	531 ± 6 (77.1 ± 0.9)	552 ± 35 (80.1 ± 5.1)
	T8	598 ± 13 (86.8 ± 1.9)	605 ± 16 (87.7 ± 2.3)

ultimate tensile stresses of the RSP alloys do not decrease as rapidly with temperature as that of 2124-T851 up to 150°C. The T8-temper ultimate tensile stresses of the RSP alloys are larger than those of 2124-T851 by approximately 30% at ambient temperature and 40% at 150°C. Ductilities of the RSP baseline and Cr-containing alloys approach that of 2124-T851 at 150°C (Figures 16 and 19).

Density-normalized yield stresses of Al-3Cu-2Li-1Mg-0.2Zr alloys in the T6 and T8 tempers are compared to those of 2124-T851 and Ti-6Al-4V in Figures 20 and 21. The T6-temper specific yield stresses of the RSP alloys are typically 43% larger than that of 2124 and 25% and 5% larger than those of Ti-6Al-4V in the mill-annealed and solution-treated-and-aged tempers, respectively, while the specific-yield-stress increments of the RSP alloys in the T8 temper, relative to those of 2124 and the two tempers of Ti-6Al-4V, are 52%, 30%, and 10%, respectively. The RSP alloys are thus highly attractive as substitutes for Ti-6Al-4V in applications up to 150°C.



GP61-0435-13-R

Figure 14. Variation with temperature of the yield stress after 100 hr exposure at temperature of (o) Al-3Cu-2Li-1Mg-0.2Zr, (□) Al-3Cu-2Li-1Mg-1Fe-1Ni-0.2Zr, and (Δ) Al-3Cu-2Li-1Mg-1.6Cr-0.2Zr. Original temper T6. (---) 2124-T851 plate (16).

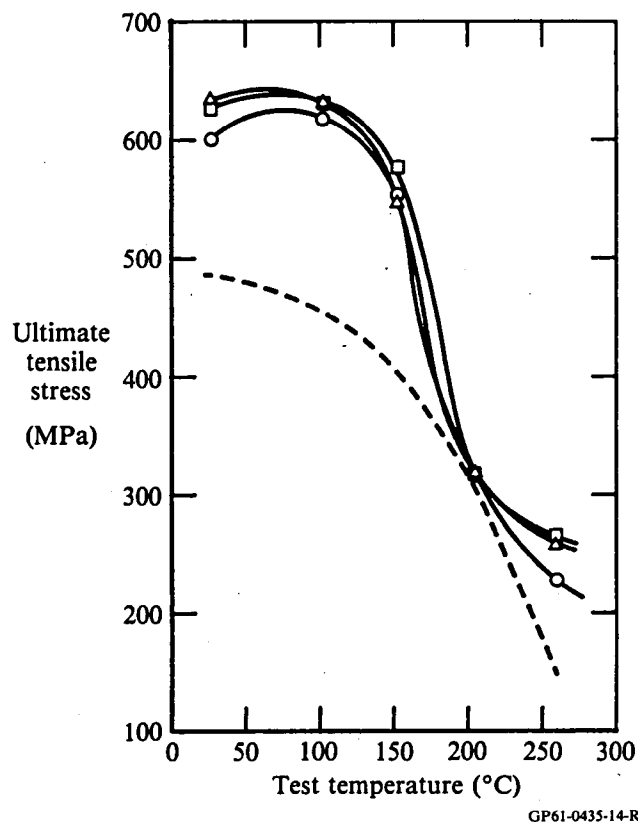


Figure 15. Variation with temperature of the ultimate tensile stress after 100 hr exposure at temperature of (○) Al-3Cu-2Li-1Mg-0.2Zr, (□) Al-3Cu-2Li-1Mg-1Fe-1Ni-0.2Zr, and (Δ) Al-3Cu-2Li-1Mg-1.6Cr-0.2Zr. Original temper T6. (---) 2124-T851 plate (16).

The addition of incoherent dispersoids to RSP Al-3Cu-2Li-1Mg-0.2Zr has a modest (~ 30 MPa) effect on strength below 150°C. The strengths of the RSP alloys decrease rapidly between 150 and 200°C and approach those of 2124-T851 at 204°C (400°F) (Figures 14, 15, 17, and 18). Above 200°C the yield and ultimate tensile stresses of the RSP alloys decrease more slowly with temperature than do those of 2124. The strength advantage afforded by the dispersoid-containing alloys is larger absolutely (up to 40 MPa) and relatively (up to 20%) at 260°C (500°F) than at lower temperatures. At this temperature, the baseline Al-3Cu-2Li-1Mg-0.2Zr-T8 alloy has a 70% larger yield stress and a 60% larger ultimate-tensile-stress than that of 2124-T851. Adding dispersoids increases the yield and ultimate tensile stress advantages of the Al-3Cu-2Li-1Mg-0.2Zr alloys relative to 2124-Al to 105% and 80%, respectively.

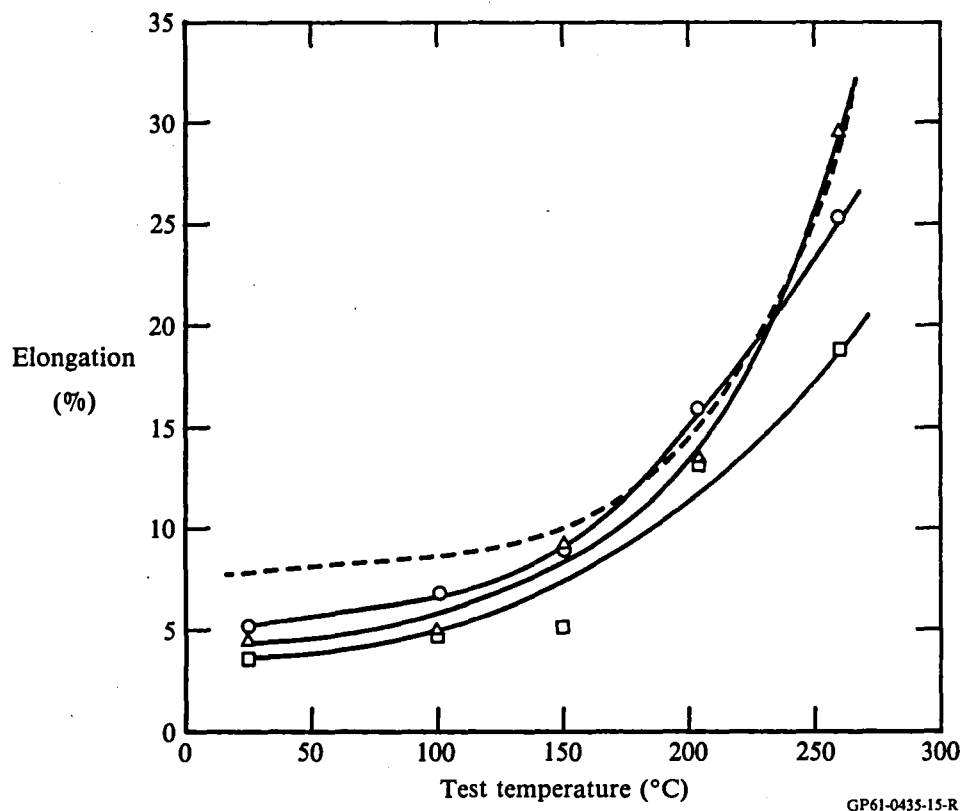
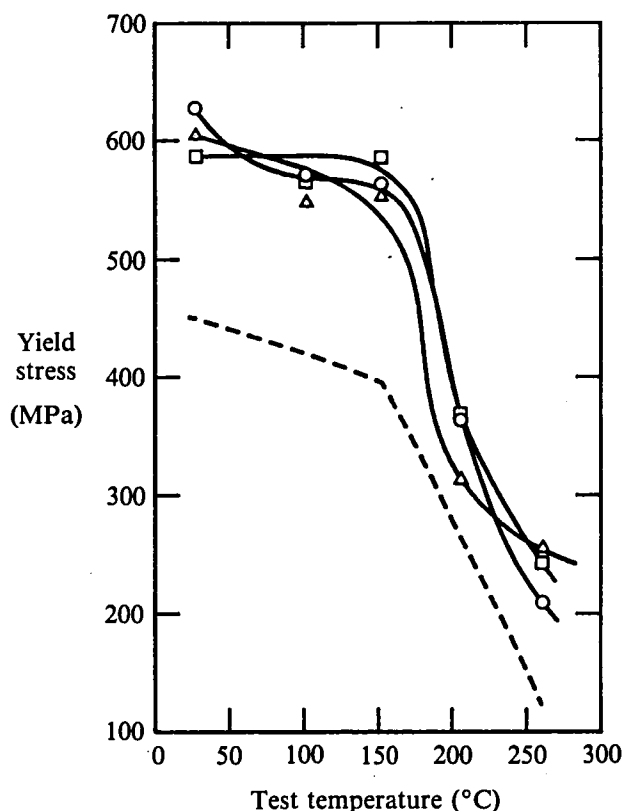


Figure 16. Variation with temperature of the ductility after 100 hr exposure at temperature of (○) Al-3Cu-2Li-1Mg-0.2Zr, (□) Al-3Cu-2Li-1Mg-1Fe-1Ni-0.2Zr, and (Δ) Al-3Cu-2Li-1Mg-1.6Cr-0.2Zr. Original temper T6. (---) 2124-T851 plate (16).

Extensive research has been performed on RSP dispersion-strengthened Al alloys such as Al-8Fe-4Ce for service to 340°C (650°F) (23,24). Interpolating the results of Sanders and Hildeman (23) at 260°C, we find that Al-8Fe-4Ce has a yield stress of 300 MPa, a density-normalized yield stress of 103 MPa cm³ g⁻¹, and 5% ductility. The RSP Al-3Cu-2Li-1Mg-1.6Cr-0.2Zr alloy at 260°C has a yield stress of 255 MPa, a density-normalized yield stress of 99 MPa cm³ g⁻¹, and 31% ductility, making it an attractive alternative to non-heat-treatable, dispersoid-rich RSP Al alloys in this temperature range for fairly short-time (< 100 hr) applications.

4.4.3 Fracture Toughness

The alloy Al-3Cu-2Li-1Mg-1.6Cr-0.2Zr was selected for fracture toughness evaluations. Because a 2% stretch after solution treatment is required to



GP61-0435-16-R

Figure 17. Variation with temperature of the yield stress after 100 hr exposure at temperature of (o) Al-3Cu-2Li-1Mg-0.2Zr, (□) Al-3Cu-2Li-1Mg-1Fe-1Ni-0.2Zr, and (Δ) Al-3Cu-2Li-1Mg-1.6Cr-0.2Zr. Original temper T8. (---) 2124-T851 plate (16).

relieve residual stresses and obtain valid toughness data, such data were determined for specimens in the T8 temper. The results were: LT orientation, $8.0 \pm 0.3 \text{ MPa } \sqrt{\text{m}}$, and TL orientation, $7.0 \pm 0.5 \text{ MPa } \sqrt{\text{m}}$. These values are sufficiently low to be valid K_{IC} data for 1.1-cm-thick extrusions. For comparison, a 4.8-cm-thick extrusion of the I/M alloy 2090-T8 (Al-2.9Cu-2.2Li-0.1Zr) has an LT K_{IC} of $27 \text{ MPa } \sqrt{\text{m}}$ and a TL K_{IC} of $16 \text{ MPa } \sqrt{\text{m}}$.

Since the major alloying-element chemistry of the RSP alloy is not very different from that of 2090, the RSP alloy's low toughness may be caused by the Cr-containing dispersoids or pre-existing inclusions and oxides. RSP Al-4Cu-1.5Mg-1Fe-1Ni-0.2Zr (1), which has 4.4 vol% Al_9FeNi dispersoids of similar size to the $\text{Al}_{18}\text{Cr}_2\text{Mg}_3$ dispersoids in the Al-3Cu-2Li-1Mg-1.6Cr-0.2Zr alloy, has an LT fracture toughness K_Q of $46 \text{ MPa } \sqrt{\text{m}}$ and a TL K_Q of $28 \text{ MPa } \sqrt{\text{m}}$. The presence of incoherent dispersoids in the RSP Cr-containing alloy would

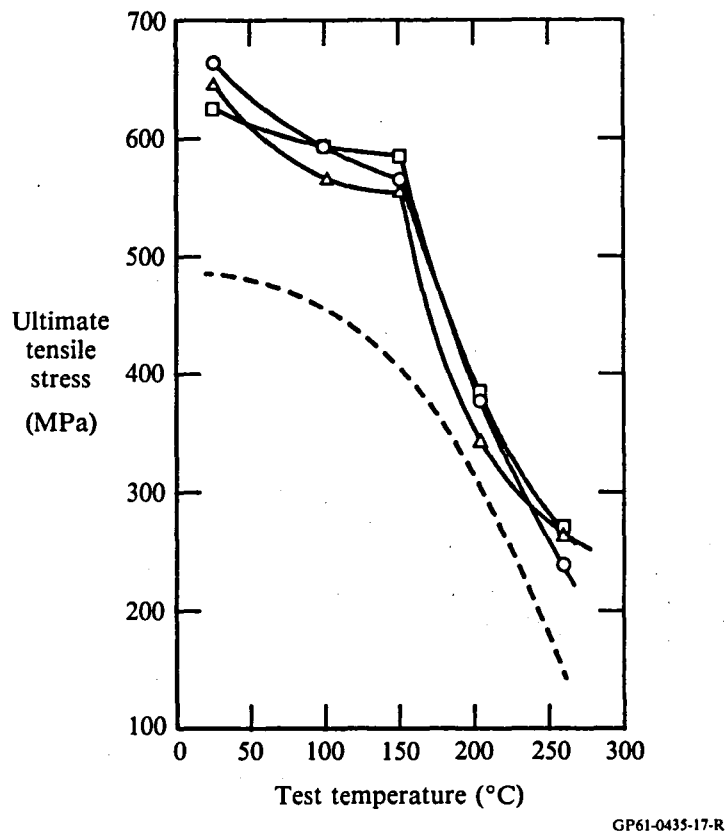
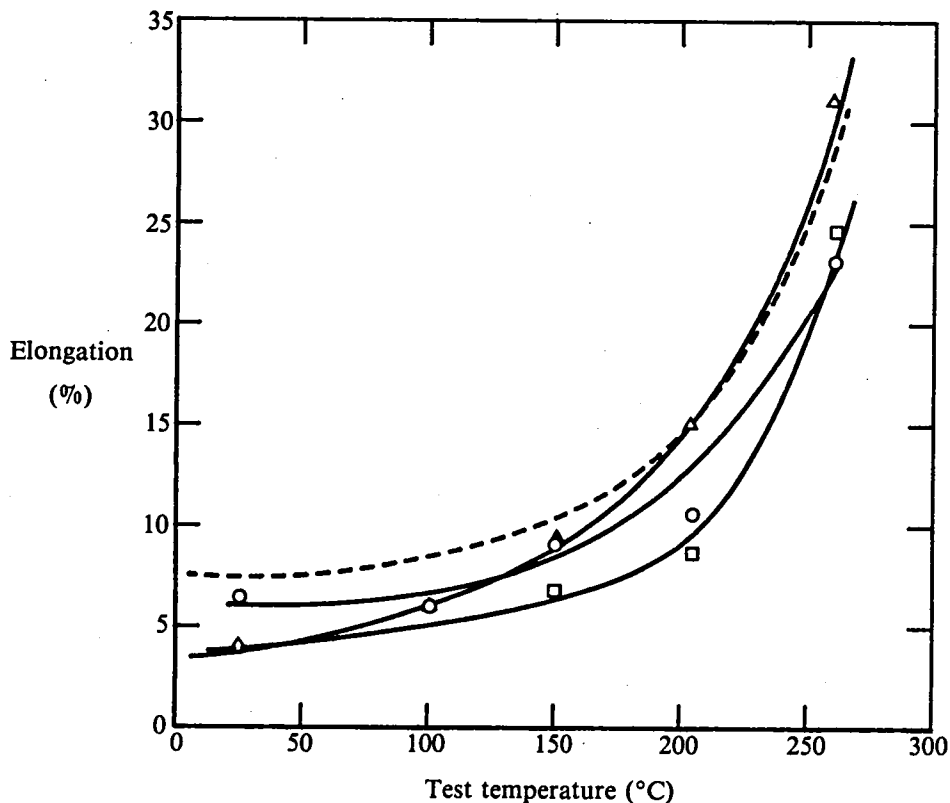


Figure 18. Variation with temperature of the ultimate tensile stress after 100 hr exposure at temperature of (○) Al-3Cu-2Li-1Mg-0.2Zr, (□) Al-3Cu-2Li-1Mg-1Fe-1Ni-0.2Zr, and (Δ) Al-3Cu-2Li-1Mg-1.6Cr-0.2Zr. Original temper T8. (---) 2124-T851 plate (16).

not, therefore, be expected to produce the observed loss in fracture toughness. The large number of inclusions, combined with the tendency towards planar slip common to all Al-Li alloys, is the most probable cause of low toughness in the RSP alloy.

4.4.4 Fatigue-Crack-Growth Rate

Fatigue-crack-growth rate (FCGR) data on Al-3Cu-2Li-1Mg-1.6Cr-0.2Zr-T8 are shown in Figure 22. Data were measured over a narrow ΔK range as a result of the low fracture toughness of the material. In contrast to previous results on RSP Al-Li alloys (1), the TL-orientation fatigue-crack-growth rate is approximately 60% smaller than the LT FCGR. This result is unexpected in view of the unrecrystallized grain structure with subgrains and oxide rows elongated in the L direction. The FCGRs are a factor of 4-7 larger than typical values for 2124-T851 plate.



GP61-0435-45-R

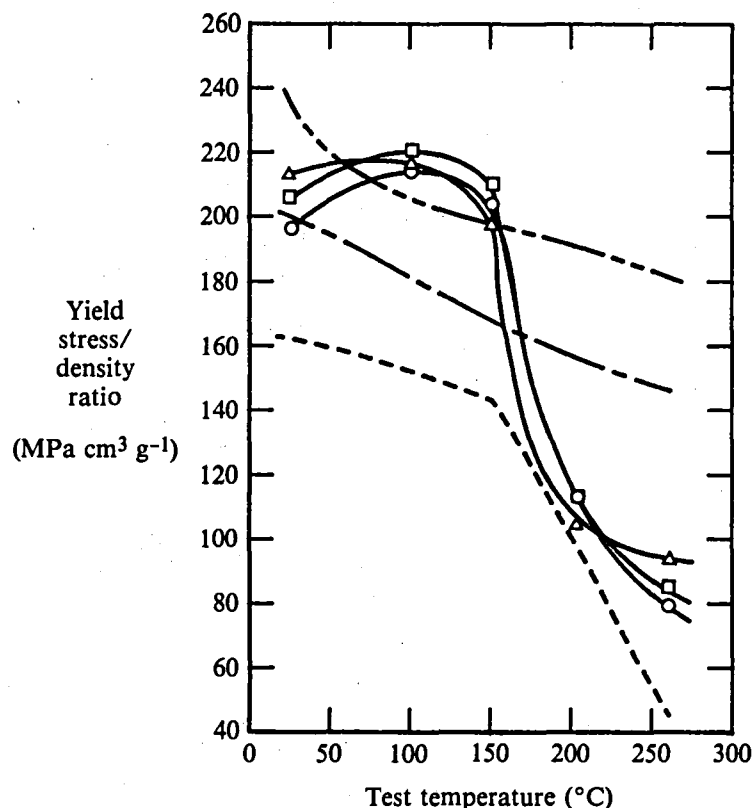
Figure 19. Variation with temperature of the ductility after 100 hr exposure at temperature of (○) Al-3Cu-2Li-1Mg-0.2Zr, (□) Al-3Cu-2Li-1Mg-1Fe-1Ni-0.2Zr, and (Δ) Al-3Cu-2Li-1Mg-1.6Cr-0.2Zr. Original temper T8. (---) 2124-T851 plate (16).

4.4.5 Creep Resistance

Creep rates of Al-3Cu-2Li-1Mg-1.6Cr-0.2Zr-T8 at 150 °C and 65, 75, and 85% of the 150°C yield stress (Figure 23) are considerably inferior to those of 2124-T851 plate. The loss in creep-rupture life increases as the relative stress level is lowered.

4.4.6 Corrosion Resistance

Weight-loss rates of the RSP alloys constantly immersed in aqueous 3.5 wt% NaCl solution for 125 hr are: Al-3Cu-2Li-1Mg-0.2Zr-T8, 0.52 mm/y; Al-3Cu-2Li-1Mg-1Fe-1Ni-0.2Zr-T8, 0.65 mm/y; and Al-3Cu-2Li-1Mg-1.6Cr-0.2Zr-T8, 0.65 mm/y. The corrosion rate is high initially and decreases with time; therefore, tests at longer exposure times are expected to yield lower corrosion rates. The



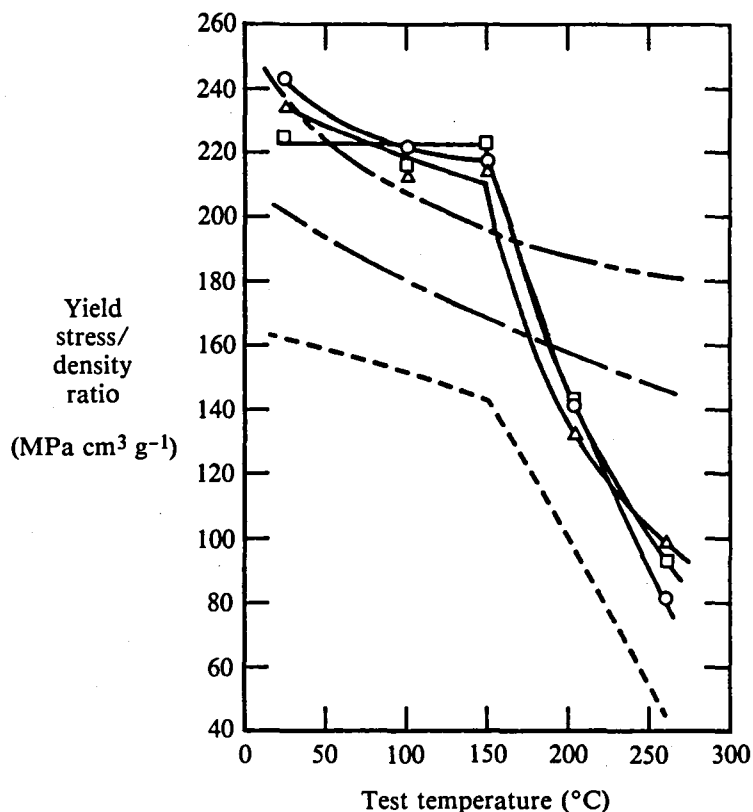
GP61-0435-18-R

Figure 20. Variation with temperature of the density-normalized yield stress after 100 hr exposure at temperature of (○) Al-3Cu-2Li-1Mg-0.2Zr-T6, (□) Al-3Cu-2Li-1Mg-1Fe-1Ni-0.2Zr-T6, (△) Al-3Cu-2Li-1Mg-1.6Cr-0.2Zr-T6, (---) 2124-T851 plate (16), (---) Ti-6Al-4V, mill annealed (15), and (---) Ti-6Al-4V, solution-treated and aged (15).

corrosion rate of 7075-T6 in natural seawater is approximately 0.09 mm/y for a 1-y test and 0.04 mm/y for a 5-y test (16). Based upon these results, it appears that the long-term corrosion resistance of the RSP alloys is lower than that of 7XXX-Al alloys.

4.5 Microstructure/Properties Correlation

The strength of the Al-3Cu-2Li-1Mg-0.2Zr alloys results from three major contributions: (1) the fine, fully-recovered substructure stabilized by coherent Al_3Zr dispersoids; (2) δ' , S' , and T_1 precipitates, with δ' being predominant in the T6 temper and S' and T_1 being predominant in the T8 temper; and (3) the Al_9FeNi or $Al_{18}Cr_2Mg_3$ incoherent dispersoids (where applicable). The importance of the various strengthening mechanisms varies with heat treatment and test temperature.

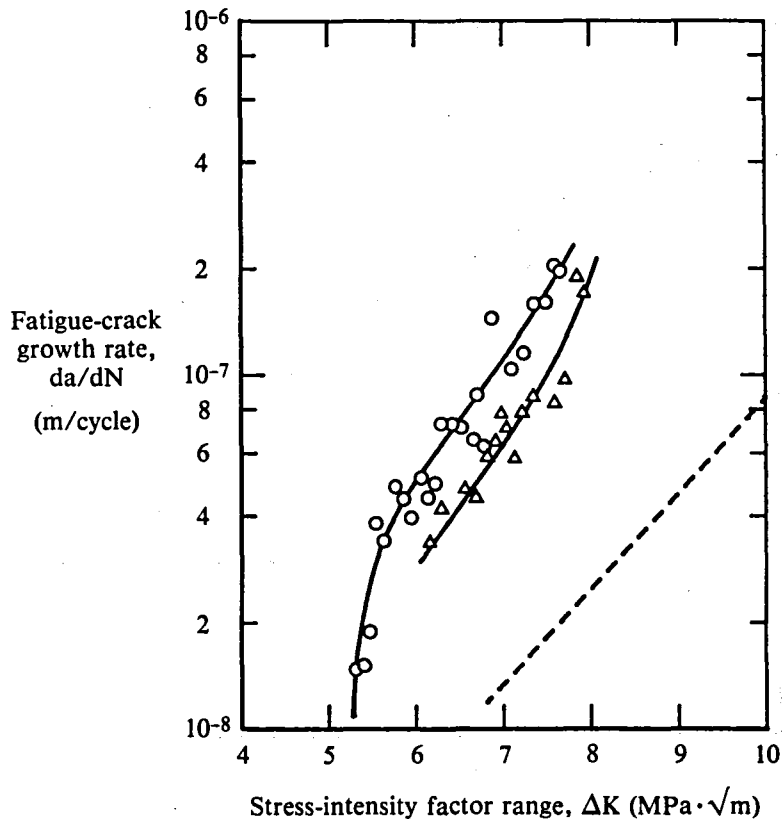


GP61-0435-19-R

Figure 21. Variation with temperature of the density-normalized yield stress after 100 hr exposure at temperature of (○) Al-3Cu-2Li-1Mg-0.2Zr-T8, (□) Al-3Cu-2Li-1Mg-1Fe-1Ni-0.2Zr-T8, (△) Al-3Cu-2Li-1Mg-1.6Cr-0.2Zr-T8, (---) 2124-T851 plate (16), (— — —) Ti-6Al-4V, mill annealed (15), and (— — —) Ti-6Al-4V, solution-treated and aged (15).

At ambient temperature, the T6 yield stress of the baseline Al-3Cu-2Li-1Mg-0.2Zr alloy is approximately 510 MPa (Table 9). The increment in yield stress caused by T_1 and S' precipitation resulting from a 2% intermediate stretch is 75-80 MPa (Table 9 and 17,21). The additional yield-stress increment resulting from dispersion-strengthening by 0.4- to 2- μ m diameter Al_9FeNi and $Al_{18}Cr_2Mg_3$ dispersoids is 20-30 MPa (Table 9).

Previous research at MDRL (8,9) on coarse- and fine-grained Al-3Li and Al-3Li-2Cu alloys indicates that the Hall-Petch strengthening contribution of 2- μ m-diameter subgrains is 80-100 MPa. Several authors (4,25,26) have estimated the strengthening contribution of δ' precipitates, which for 3 wt% Li is approximately 150-200 MPa (4). Contributions to the overall strength of multicomponent Al-Cu-Li-Mg-Zr alloys, resulting from Cu and Mg solid-solution strengthening and T_1 and S' precipitation, have not been predicted theoretically.



GP61-0435-20-R

Figure 22. FCGR results on Al-3Cu-2Li-1Mg-1.6Cr-0.2Zr, T8 temper: (○) LT orientation, (Δ) TL orientation, and (— —) typical results for 2124-T851 (16).

The measured dispersion-strengthening contribution is relatively small and is equal to that provided by Al₉FeNi dispersoids in RSP Al-4.4Cu-1.5Mg-1Fe-1Ni-0.2Zr and calculated using the Orowan theory (1). As in the previous study (1), the solidification rate was insufficiently high to produce an as-solidified dispersoid distribution corresponding to significant Orowan strengthening. The production of insoluble Al₁₈Cr₂Mg₃ rather than soluble Al₇Cr dispersoids during consolidation processing obviated the possibility of tailoring the distribution of Cr-containing dispersoids to improve the strength significantly.

Several investigators (27-29) have determined yield stresses of Al-Li alloys, with and without Cu and Zr, between ambient temperature and 300°C. Coarse-grained alloys not containing Zr had low (300 MPa) yield stresses at 25°C which were maintained up to approximately 200°C. Fine-grained Al-Li-Zr and Al-Li-Mg-Zr alloys had high (450 MPa) yield stresses at 25°C which

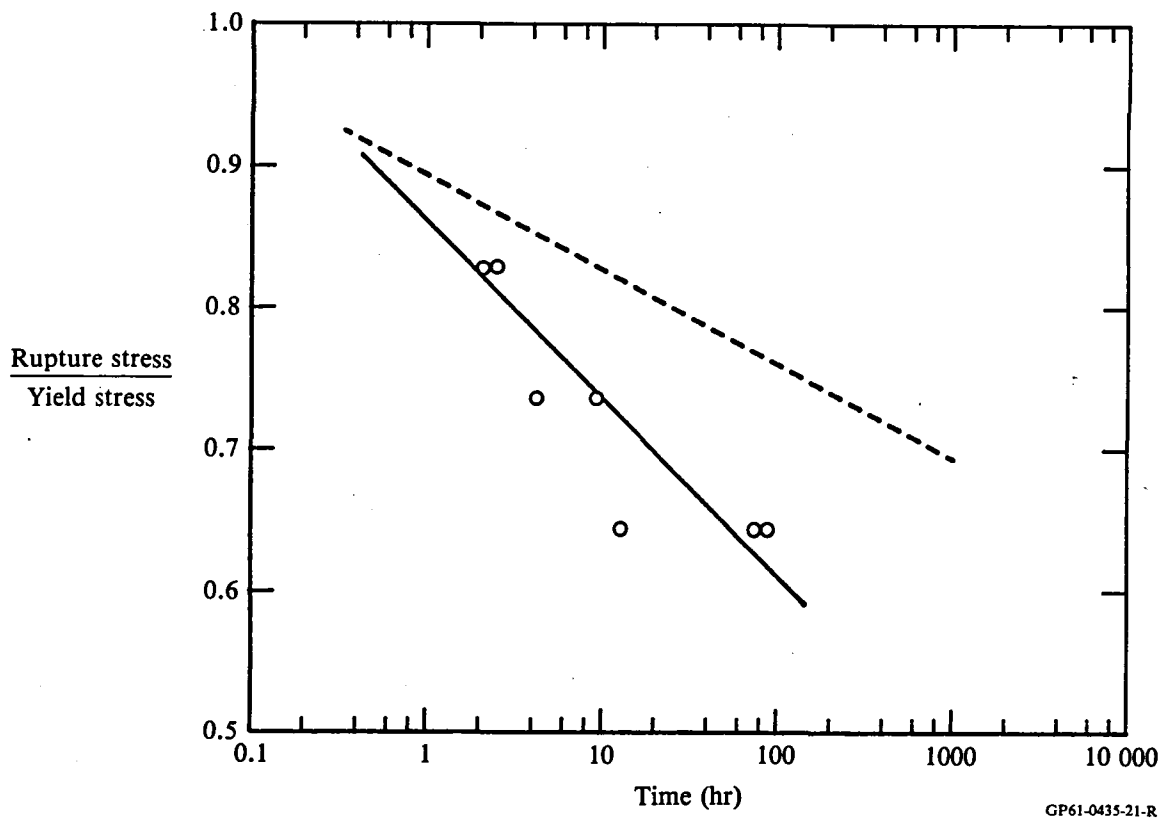


Figure 23. 150°C creep-test results for (o) Al-3Cu-2Li-1Mg-1.6Cr-0.2Zr-T8 and (---) typical results for 2124-T851 (16).

decreased rapidly above 50-75°C. The strength decrease was attributed to dynamic recovery caused by the movement of dislocations to sub-boundaries during deformation. Al-Li-Cu-Zr and Al-Li-Cu-Mg-Zr alloys maintained much of their strength to 150°C. Strength retention was attributed to formation of constituent phases such as S and T₂ at sub-boundaries which acted as dislocation sinks and prevented dynamic recovery. The Cu-containing alloys showed strength increases up to 100°C as the result of additional δ' precipitation during elevated-temperature exposure (29).

The RSP Al-3Cu-2Li-1Mg-0.2Zr alloys studied here have elevated-temperature deformation behavior similar to that of the Cu-containing alloys mentioned above, except that strength retention in the 100-150°C range is better than in the lower-Cu alloys studied by Sastry and O'Neal (Al-3Li-1.5Cu-0.5Co-0.2Zr) (28) and Pridham *et al.* (Al-2.5Li-1.7Cu-0.7Mg-0.12Zr) (29). The additional strength retention results from a larger volume fraction and more extensive precipitation of Cu-containing particles in the present alloys.

The strengthening precipitates coarsen rapidly and the yield stress decreases rapidly upon elevated-temperature exposure above 150°C. Much of the yield stress above 200°C is contributed by T_1 , T_2 , and S particles on sub-boundaries. Since particle spacings are fixed by the subgrain diameter, particles in the RSP alloys are typically smaller and more closely spaced than in I/M 2124, leading to higher strength above 200°C. Since the overall yield stress has decreased from 580-600 MPa at ambient temperature to 200-250 MPa at 260°C, the temperature-insensitive strengthening contribution from insoluble [Fe + Ni]- and Cr-containing dispersoids becomes significant. The favorable 260°C strength of these alloys relative to Al-8Fe-4Ce may result from smaller, more closely spaced particles of all types than are present in the latter alloy.

The sharp decrease in fracture toughness and fatigue-crack-growth rate of Al-3Cu-2Li-1Mg-1.6Cr-0.2Zr relative to 2090-Al is presumed to result from the high inclusion count in the RSP alloy. Ductilities in both longitudinal and long-transverse specimens are similar to those measured for Al-3Li-Cu alloys (8,9), which had considerably smaller inclusion concentrations. Recent IRAD at MDRL (30) has shown that production of a 99% dense preform by deposition of molten Al-4Li-1Cu-0.2Zr droplets onto a substrate, followed by forging and rolling to sheet, produced a material with 20 ppm oxygen. In comparison, material with 500 ppm oxygen was produced in a sheet rolled from a powder-metallurgical extrusion. The low-oxygen sheet had improved ductility and notch-tensile stress/yield-stress ratio resulting from the lower volume fraction of inclusions and oxide particles. Reduction of oxide concentrations in the alloys studied here would provide the potential for similar improvements in ductility and toughness.

The grain structure of the RSP Al-3Cu-2Li-1Mg-1.6Cr-0.2Zr alloy, solution-treated and aged, is a mixture of low- and high-angle grain boundaries. The density of high-angle boundaries is higher than that of commercial I/M aluminum alloys because of the small grain size. These high-angle boundaries may serve as easy diffusion paths, thereby enhancing diffusional creep and reducing the creep-rupture lifetime relative to that of an I/M alloy such as 2124. Short creep lifetimes may thus be an inherent property of RSP Al alloys.

The high corrosion rates reported here are in agreement with recent work (10) which has shown that the corrosion resistance of Al-Li alloys is primarily influenced by the Cu concentration and is not strongly related to Li concentration or heat treatment. High-Cu non-Li-containing alloys such as 2024-Al have similarly low corrosion resistances (16). Such alloys are normally clad to produce acceptable corrosion behavior in service, and it is assumed that RSP high-Cu Al-Li alloys would require the same treatment.

**5. TASK 6: LOW-DENSITY AL-4Li-Cu-Mg-Zr ALLOYS
FOR AMBIENT-TEMPERATURE APPLICATIONS**

5.1 Alloy Composition

Concentrations of major alloying elements in the three Al-4Li-Cu-Mg-Zr alloys are listed in Table 10. Nominal and analyzed concentrations are equivalent in all cases. Hydrogen concentrations are at most 1 ppm larger and oxygen concentrations are significantly lower in the Al-4Li alloys than in the Al-3Cu-2Li-1Mg-0.2Zr alloys (Table 3). This result is surprising in view of the reactivity of Al-high Li powders, and testifies to the efficacy of the selected degassing and consolidation processing cycle in removing H and O impurities.

5.2 Microstructure

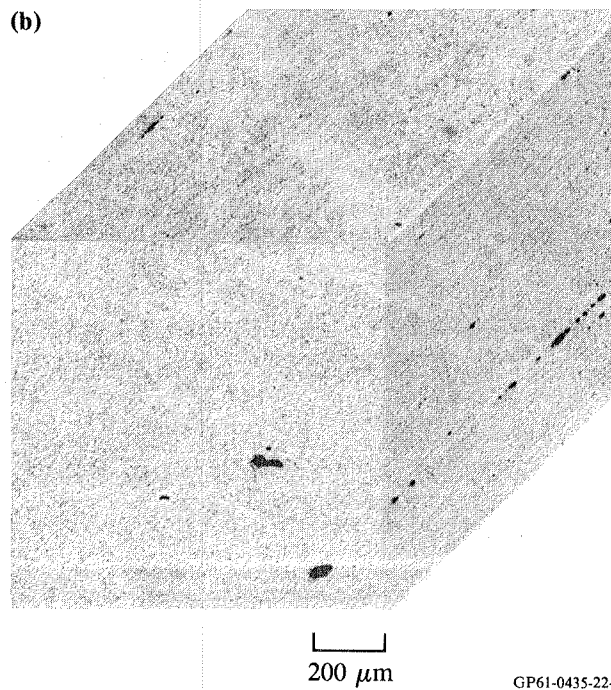
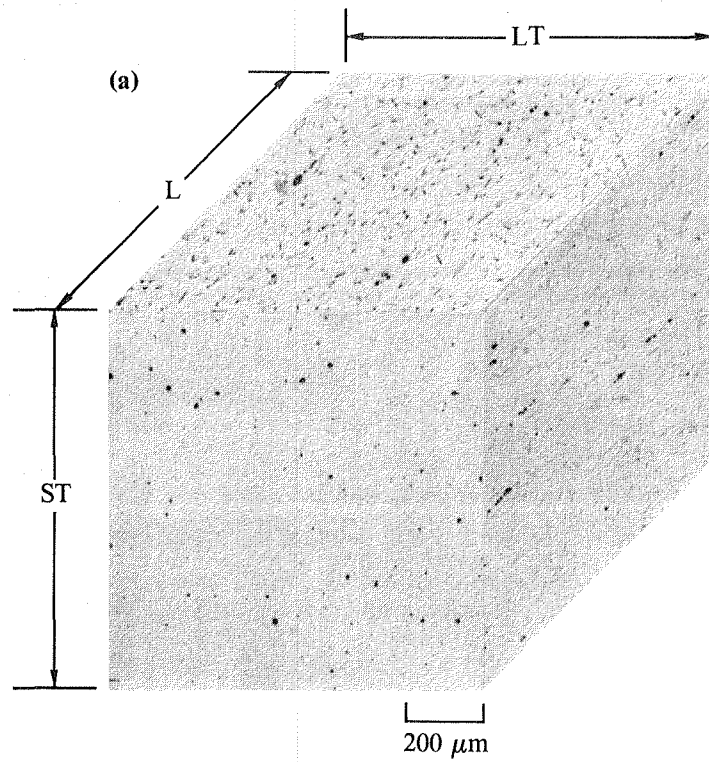
5.2.1 Evaluation of Inclusions

Optical photomicrographs of unetched sections of solution-treated Al-4Li-Cu-Mg-Zr alloys (Figure 24) reveal distributions of inclusions similar in size and density to those observed in Al-3Cu-2Li-1Mg-0.2Zr alloys (Figure 7). The presence of inclusions is expected to have deleterious effects on transverse properties and toughness similar to those in the Al-3Cu-2Li-1Mg-0.2Zr alloys.

TABLE 10. COMPOSITIONS OF RSP Al-4Li-Cu-Mg-Zr ALLOYS.

Nominal composition	Analyzed composition					
	Weight %				Weight ppm	
	Li	Cu	Mg	Zr	O	H
Al-4Li-1Cu-1Mg-0.2Zr	4.0	0.99	1.11	0.22	160 ± 40	2.7
Al-4Li-0.5Cu-1.5Mg-0.2Zr	4.1	0.46	1.56	0.21	130 ± 110	2.8
Al-4Li-1.5Cu-0.5Mg-0.2Zr	4.0	1.45	0.58	0.20	105 ± 90	2.8
Al-3Li-1.5Cu-1Mg-0.5Co-0.2Zr (Ref. 1)	—	—	—	—	480 ± 60	< 20

GP61-0435-38-R



GP61-0435-22-R

Figure 24. Optical photomicrographs of unetched samples of (a) Al-4Li-1Cu-1Mg-0.2Zr and (b) Al-4Li-0.5Cu-1.5Mg-0.2Zr extrusions, solution-treated 560°C/hr.

5.2.2 As-Extruded Condition

Optical photomicrographs of as-extruded Al-4Li-Cu-Mg-Zr alloys are shown in Figure 25. The 1- to 20- μ m-diameter, dark constituent particles in Figures 25a and 25c are T_2 according to the phase diagram (20). The ~ 1- μ m-diameter constituent particles in Al-4Li-0.5Cu-1.5Mg-0.2Zr are δ or Al_2LiMg according to the Al-Li-Mg phase diagram (20). The δ phase may also be present in Figures 25a and 25c, but is difficult to differentiate from oxides because of its etching behavior. The alloys are unrecrystallized and have subgrain microstructures, as in the case of the Al-3Cu-2Li-1Mg-0.2Zr alloys. X-ray diffraction patterns of as-extruded Al-4Li alloys (Table 11) show the constituent phase δ and weak lines which may correspond to the other constituent phases mentioned above.

5.2.3 Solution-Treated Condition

The combined [Li + Cu + Mg] concentration is in excess of the equilibrium solubility limit for all three Al-4Li alloys at the maximum solution-treatment temperature of 560°C. Optical photomicrographs of Al-4Li alloys (Figure 26) show dissolution of most of the Cu and Mg, and coarsening of the remaining Cu-containing constituent particles to plates which are up to 50 μ m long (Figures 26a and 26c). These particles are expected to be detrimental to ductility and fracture toughness, as discussed by Quist *et al.* (31) with respect to RSP Al-3.7Li-2.4Cu-1.6Mg-0.2Zr. The Al_2LiMg constituent particles in Al-4Li-0.5Cu-1.5Mg-0.2Zr (Figure 26b) remain fine (1- to 2- μ m diameter) and should

**TABLE 11. CONSTITUENT AND DISPERSED PHASES
IN AS-EXTRUDED AND SOLUTION-TREATED
Al-4Li-Cu-Mg-Zr ALLOYS.**

Alloy composition	Phases present in indicated condition	
	As-extruded	Solution-treated 560°C/1 h
Al-4Li-1Cu-1Mg-0.2Zr	δ (AlLi), others	Peak intensities too small for identification
Al-4Li-0.5Cu-1.5Mg-0.2Zr	δ (AlLi), others	Al_2LiMg
Al-4Li-1.5Cu-0.5Mg-0.2Zr	δ (AlLi), others	Peak intensities too small for identification

GP61-0435-39-R

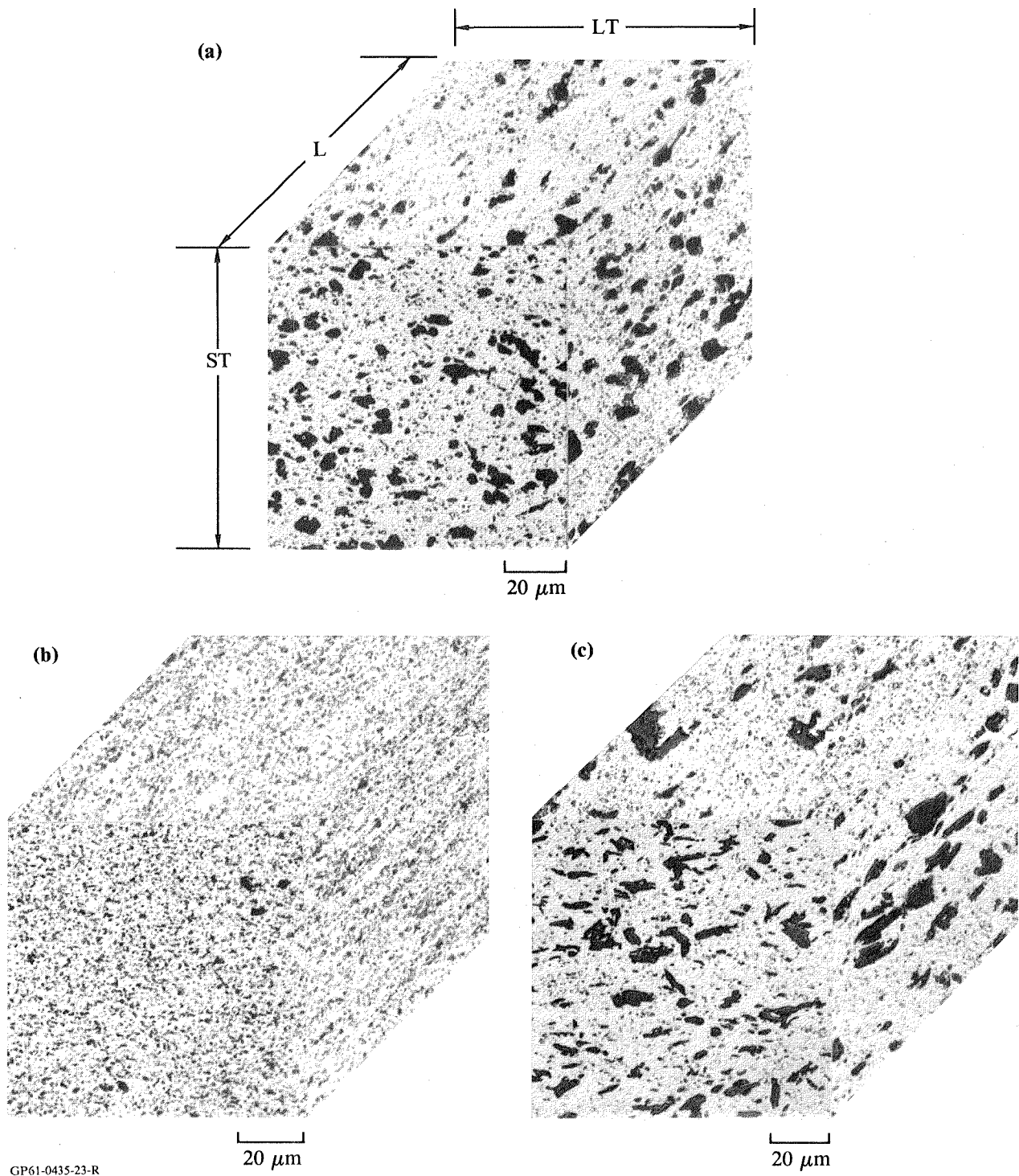


Figure 25. Optical photomicrographs of as-received extrusions of (a) Al-4Li-1Cu-1Mg-0.2Zr, (b) Al-4Li-0.5Cu-1.5Mg-0.2Zr, and (c) Al-4Li-1.5Cu-0.5Mg-0.2Zr.

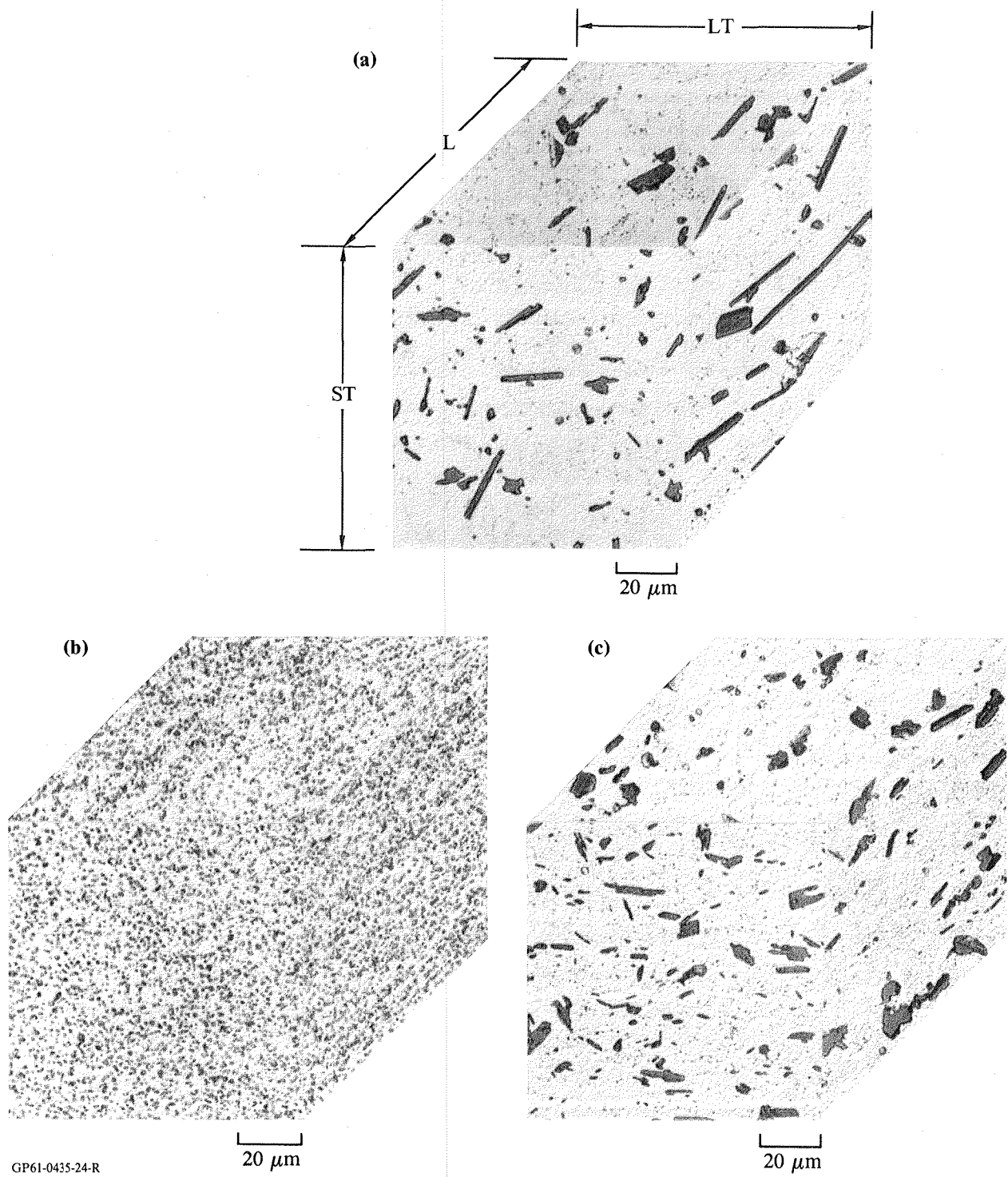


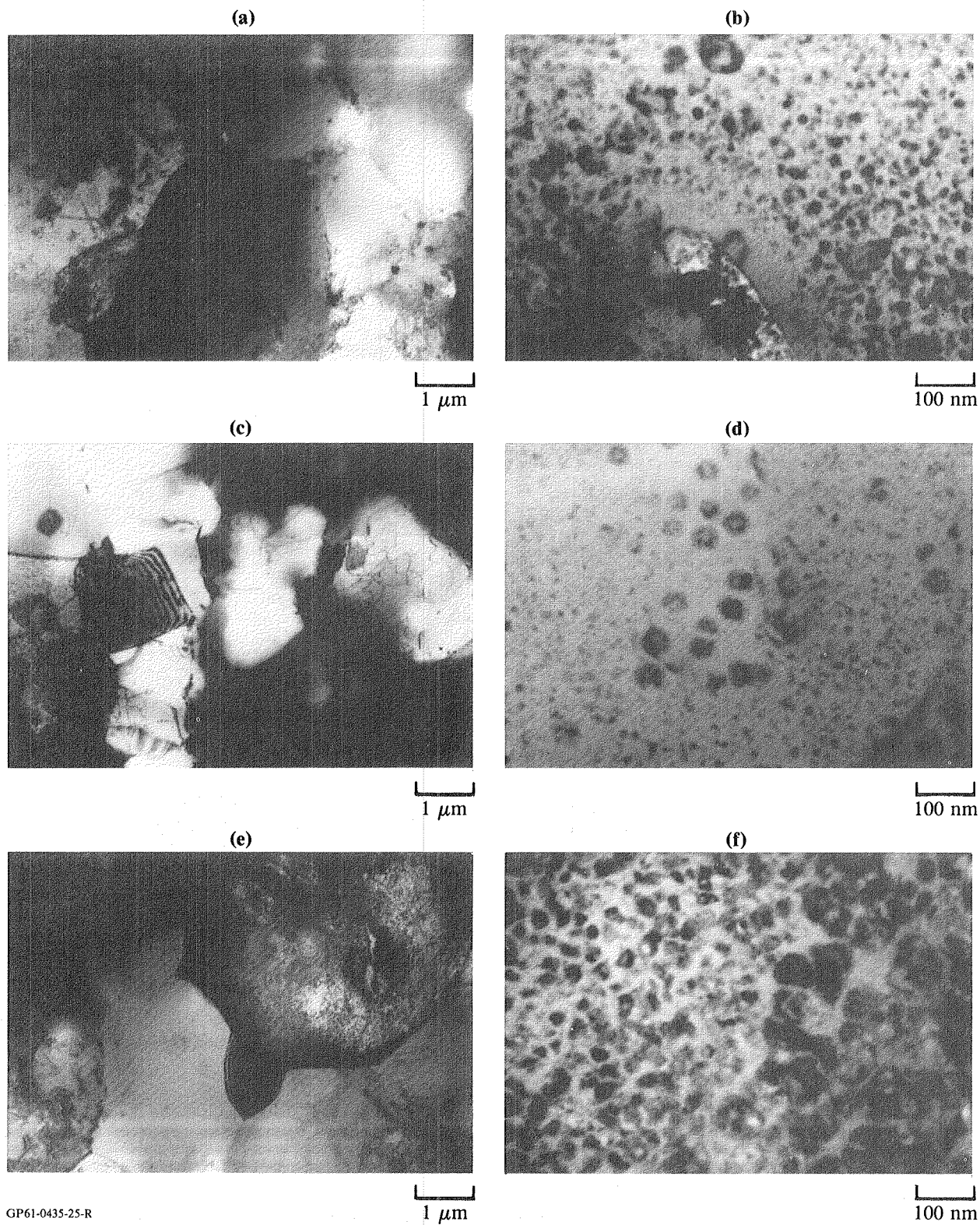
Figure 26. Optical photomicrographs of (a) Al-4Li-1Cu-1Mg-0.2Zr, (b) Al-4Li-0.5Cu-1.5Mg-0.2Zr, and (c) Al-4Li-1.5Cu-1.5Mg-0.2Zr extrusions, solution-treated at 560°C for 1 hr.

not have as deleterious an effect on properties as the Cu-containing constituent particles. X-ray diffraction patterns (Table 11) confirm the presence of Al_2LiMg in Figure 26b, but do not identify the Cu-containing constituent particles, owing to their small volume fractions.

Grain/subgrain sizes in solution-treated Al-4Li alloys are evaluated from transmission electron micrographs (Figure 27). Geometric mean subgrain diameters of the three alloys are: Al-4Li-1Cu-1Mg-0.2Zr, 2.5 μm ; Al-4Li-0.5Cu-1.5Mg-0.2Zr, 2.5 μm ; and Al-4Li-1.5Cu-0.5Mg-0.2Zr, 2.0 μm . The lithium supersaturation in Al-4Li alloys is such that δ' precipitation cannot be suppressed by water quenching from 560°C (Figures 27b, 27d, 27f). Many of the precipitates are doughnut-shaped and lack sharp boundaries. This may reflect formation of composite $\text{Al}_3(\text{Li},\text{Zr})$ precipitates as reported by Malis (32) and Gayle and Vandersande (33), or decomposition of the Al-rich solid solution via a low-temperature miscibility gap as predicted by Sigli and Sanchez (34) and reported by Papazian *et al.* (35). Most of the doughnut-shaped precipitates disappear upon subsequent aging at 160°C.

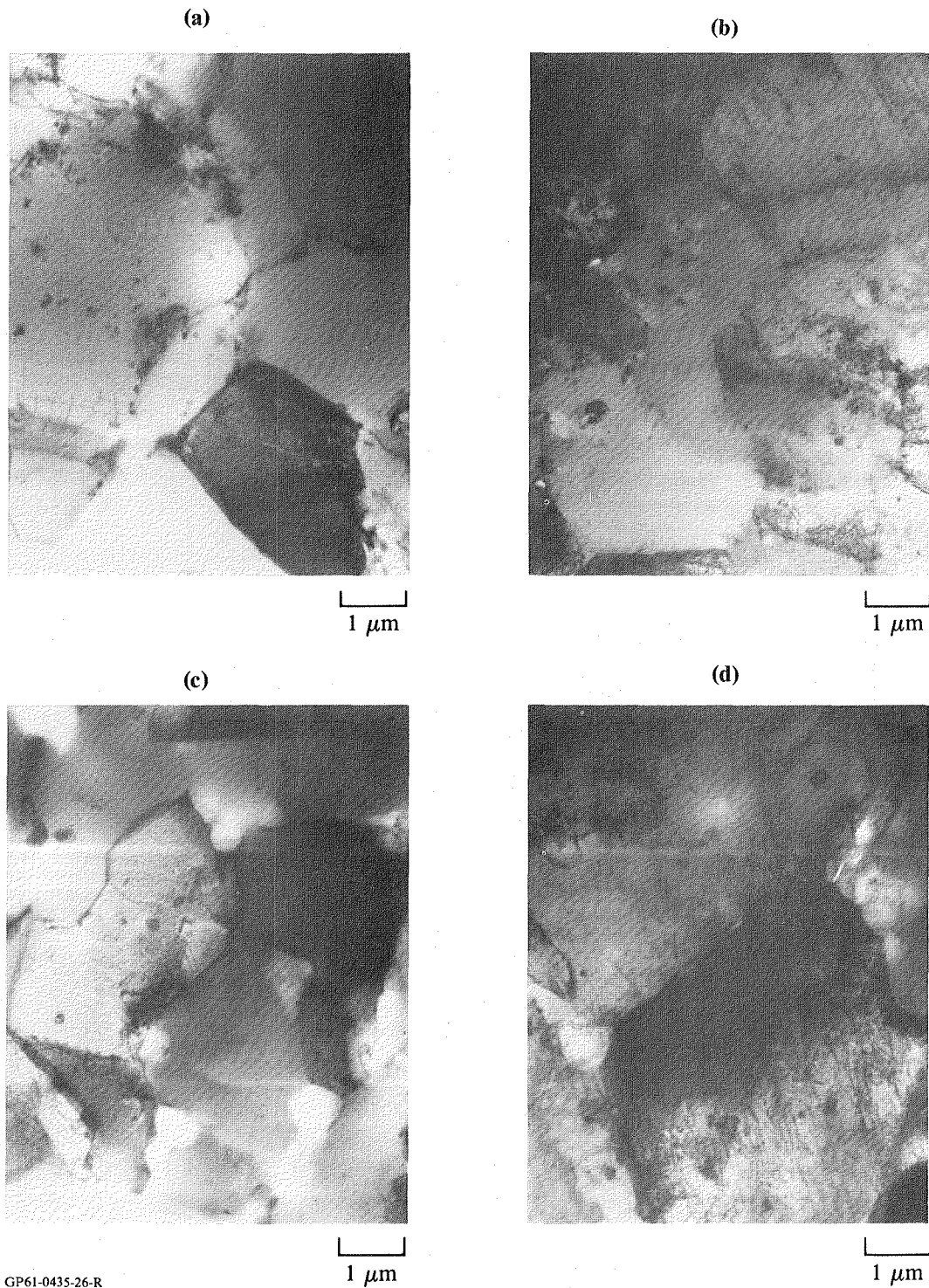
5.2.4 Aged Condition

Transmission electron photomicrographs of Al-4Li-Cu-Mg-0.2Zr alloys peak-aged at 160°C reveal few differences between the T6 and T8 tempers (Figure 28). The 2% intermediate stretch in the T8 samples is accommodated by planar slip in some grains (e.g., upper left in Figure 28b, right of center in Figure 28d) and by dislocation tangling near subgrain boundaries in others (e.g., upper right in Figure 28b, far left in Figure 28d). Precipitated phases other than δ' are not observed even in the Cu-rich alloy in the T8 temper, and the intermediate stretch does not alter the morphology or size of δ' precipitates (compare Figures 28f and 28h). The Cu not present in constituent particles is in solid solution in these alloys, which have high Li:Cu ratios, rather than in T_1 or S' precipitates.



GP61-0435-25-R

Figure 27. Transmission electron photomicrographs of 560°C solution-treated and quenched (a), (b) Al-4Li-1Cu-1Mg-0.2Zr, (c), (d) Al-4Li-0.5Cu-1.5Mg-0.2Zr, and (e), (f) Al-4Li-1.5Cu-0.5Mg-0.2Zr.



GP61-0435-26-R

Figure 28. Transmission electron photomicrographs of RSP Al-4Li alloys, solution treated 560°C/1 hr and aged 160°C/48 hr (T6), or solution-treated 560°C/1 hr, stretched 2%, and aged 160°C/48 hr (T8). (a), (b) Al-4Li-1Cu-1Mg-0.2Zr; (a) T6, (b) T8; (c), (d) Al-4Li-0.5Cu-1.5Mg-0.2Zr; (c) T6, (d) T8; (e) - (h) Al-4Li-1.5Cu-0.5Mg-0.2Zr; (e), (f) T6; (g), (h) T8.

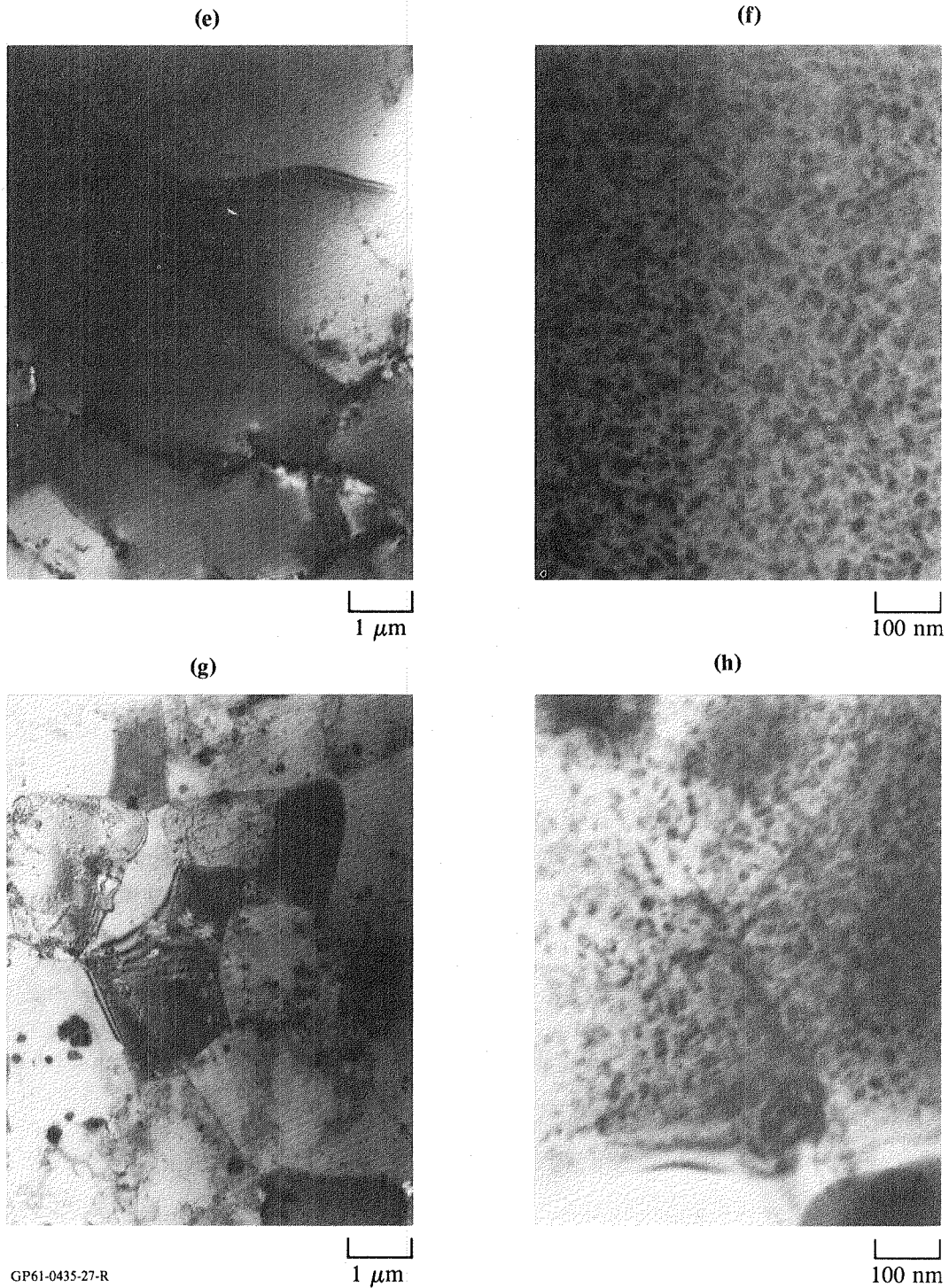


Figure 28. (Continued) Transmission electron photomicrographs of RSP Al-4Li alloys, solution treated 560°C/1 hr and aged 160°C/48 hr (T6), or solution-treated 560°C/1 hr, stretched 2%, and aged 160°C/48 hr (T8). (a), (b) Al-4Li-1Cu-1Mg-0.2Zr; (a) T6, (b) T8; (c), (d) Al-4Li-0.5Cu-1.5Mg-0.2Zr; (c) T6, (d) T8; (e) - (h) Al-4Li-1.5Cu-0.5Mg-0.2Zr; (e), (f) T6; (g), (h) T8.

5.3 Properties

5.3.1 Density and Elastic Modulus

Densities of the Al-4Li-Cu-Mg-Zr alloys listed in Table 12 show the expected 14-14.5% decrease relative to 7075-Al, consistent with densities of Al-4Li-Mg-Zr and Al-4Li-Cu-Zr alloys (10). The density decreases slightly with decreasing Cu:Mg ratio as expected. Elastic moduli of these alloys show considerable scatter, but typical values are ~ 86 GPa (12.5×10^6 psi). Quist (31) reported a modulus of 82.7 GPa (12×10^6 psi) for RSP Al-3.7Li-2.4Cu-1.6Mg-0.2Zr, which is consistent with the value reported here when the differing Li contents of the alloys are taken into account. The modulus/density ratios of the RSP Al-4Li alloys are about $36 \text{ GPa cm}^3 \text{ g}^{-1}$, or 44% larger than the ratio of $25 \text{ GPa cm}^3 \text{ g}^{-1}$ typical of 7XXX-Al alloys.

5.3.2 Mechanical Properties

Ambient-temperature tensile properties of Al-4Li-Cu-Mg-Zr alloys in the T6 and T8 tempers are listed in Table 13. The yield stresses of all alloys are 480 ± 10 MPa, independent of composition and heat treatment. Yield stresses are approximately 10 MPa larger, on average, than those of Al-4Li-1Cu-0.2Zr and Al-4Li-1Mg-0.2Zr (Table 2). The 2% intermediate stretch increases the ultimate tensile stress by about 30 MPa in all three alloys, and has a small beneficial effect on the ductility. Ductilities are similar to those of peak-aged Al-4Li-1Cu-0.2Zr and Al-4Li-1Mg-0.2Zr reported in Table 2, and are superior to those of peak-aged RSP Al-4Li-2Cu-0.2Zr and Al-4Li-2Mg-0.2Zr, which consistently failed prior to yielding. The Al-4Li-0.5Cu-1.5Mg-0.2Zr alloy is equivalent in strength to 7050-T76511 and has a 14.5% lower density;

**TABLE 12. MASS DENSITIES OF
Al-4Li-Cu-Mg-Zr ALLOYS.**

Alloy composition	Mass density (g/cm ³)	% reduction relative to 7075-Al
Al-4Li-1Cu-1Mg-0.2Zr	2.402	14.2
Al-4Li-0.5Cu-1.5Mg-0.2Zr	2.394	14.5
Al-4Li-1.5Cu-0.5Mg-0.2Zr	2.409	14.0

GP61-0435-40-R

TABLE 13. AMBIENT-TEMPERATURE MECHANICAL PROPERTIES OF PEAK-AGED Al-4Li-Cu-Mg-0.2Zr ALLOYS.

Alloy composition	Temper	Yield stress (MPa [ksi])	Ultimate tensile stress (MPa [ksi])	Elongation (%)
Al-4Li-1Cu-1Mg-0.2Zr	T6	487 ± 8 (70.7 ± 1.2)	499 ± 8 (72.4 ± 1.2)	4.5 ± 0.4
	T8	481 ± 17 (69.7 ± 2.5)	526 ± 29 (76.3 ± 4.2)	5.0 ± 2.1
Al-4Li-0.5Cu-1.5Mg-0.2Zr	T6	482 ± 4 (70.0 ± 0.6)	526 ± 9 (76.3 ± 1.3)	2.4 ± 0.5
	T8	488 ± 12 (70.7 ± 1.8)	556 ± 12 (80.6 ± 1.7)	4.2 ± 0.8
Al-4Li-1.5Cu-0.5Mg-0.2Zr	T6	477 ± 16 (69.1 ± 2.3)	481 ± 10 (69.7 ± 1.5)	3.0 ± 1.2
	T8	468 ± 13 (67.8 ± 1.9)	510 ± 13 (74.0 ± 1.9)	3.4 ± 0.6

GP61-0435-41-R

thus it is an attractive substitute for 7XXX-Al alloys, provided that the ductility and fracture toughness can be increased to competitive levels.

Long-transverse yield stresses (Table 14) are equivalent to longitudinal yield stresses, but ductility is severely degraded, with only the Al-4Li-0.5Cu-1.5Mg-0.2Zr alloy not failing prior to yielding. Compressive yield stresses of the Al-4Li alloys (Table 15) are equivalent to the tensile yield stresses in three of six cases and are superior by 25-40 MPa in the other three cases. The source of this behavior is not well understood, since only δ' precipitates form and the precipitate morphology and distribution are not sensitive to intermediate stretch.

5.3.3 Fracture Toughness

The alloy Al-4Li-1Cu-1Mg-0.2Zr-T8 was selected for fracture toughness evaluations. The results are 9.5 ± 0.3 MPa \sqrt{m} for the LT orientation, and 7.5 ± 0.4 MPa \sqrt{m} for the TL orientation. These values are valid K_{IC} data for 1.1-cm-thick extrusions. Since the fracture toughnesses of these alloys are slightly higher than those of Al-3Cu-2Li-1Mg-1.6Cr-0.2Zr-T8, the low values are probably related to the presence of a relatively large volume-fraction of brittle inclusions and not to the high Li level.

TABLE 14. AMBIENT-TEMPERATURE LONG-TRANSVERSE MECHANICAL PROPERTIES OF PEAK-AGED Al-4Li-Cu-Mg-0.2Zr ALLOYS.

Alloy composition	Temper	Yield stress (MPa [ksi])	Ultimate tensile stress (MPa [ksi])	Elongation (%)
Al-4Li-1Cu-1Mg-0.2Zr	T6	474 ± 3 (68.7 ± 0.4)	—*	0.7 ± 0.1 —
Al-4Li-0.5Cu-1.5Mg-0.2Zr	T6	484 ± 4 (70.2 ± 0.6)	502 ± 8 (72.8 ± 1.1)	1.5 ± 0.3
Al-4Li-1.5Cu-0.5Mg-0.2Zr	T6	480 ± 6 (69.6 ± 0.9)	—*	0.9 ± 0.2 —

*All specimens failed prior to yield

GP63-0435-42-R

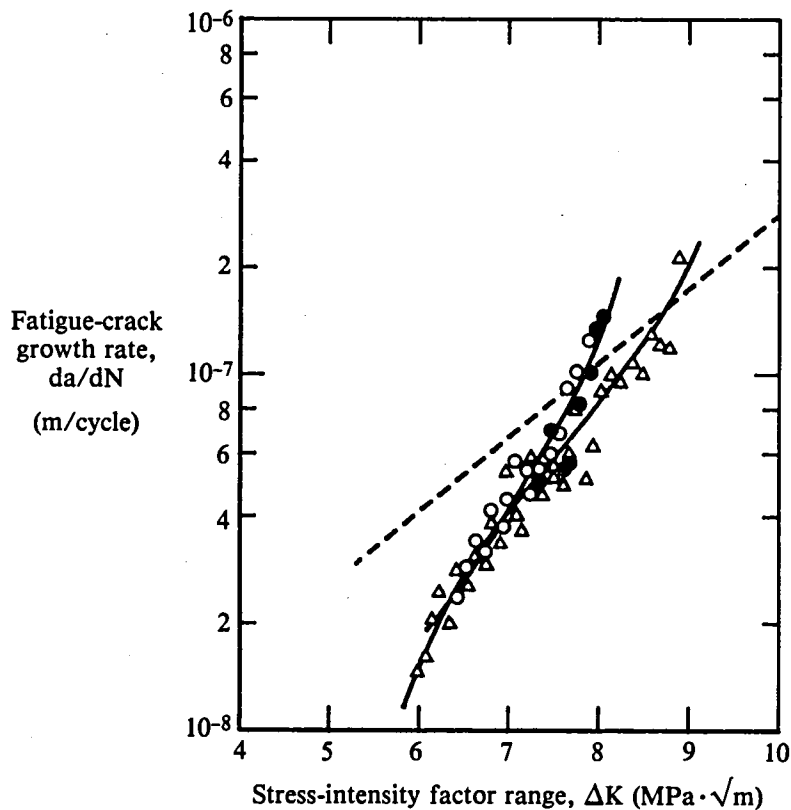
TABLE 15. AMBIENT-TEMPERATURE COMPRESSIVE YIELD STRESSES OF RSP Al-4Li-Cu-Mg-0.2Zr ALLOYS

Alloy composition	Temper	Compressive yield stress (MPa [ksi])	Tensile yield stress (MPa [ksi])
Al-4Li-1Cu-1Mg-0.2Zr	T6	486 ± 12 (70.4 ± 1.7)	487 ± 8 (70.7 ± 1.2)
	T8	488 ± 5 (70.7 ± 0.7)	481 ± 17 (69.7 ± 2.5)
Al-4Li-0.5Cu-1.5Mg-0.2Zr	T6	487 ± 3 (70.7 ± 0.4)	482 ± 4 (70.0 ± 0.6)
	T8	510 ± 4 (73.9 ± 0.5)	488 ± 12 (70.7 ± 1.8)
Al-4Li-1.5Cu-0.5Mg-0.2Zr	T6	502 ± 6 (72.9 ± 0.8)	477 ± 16 (69.1 ± 2.3)
	T8	509 ± 3 (73.8 ± 0.4)	468 ± 13 (67.8 ± 1.9)

GP61-0435-43-R

5.3.4 Fatigue-Crack-Growth Rate

Fatigue-crack-growth rate (FCGR) data on Al-4Li-1Cu-1Mg-0.2Zr-T8 are shown in Figure 29. Crack-growth rates in LT and TL orientations are similar over the small ΔK range of measurement. The FCGR falls below that of 7075-T6 in the threshold region, and the engineering stress-intensity factor threshold is approximately 5 MPa \sqrt{m} .



GP61-0435-28-R

Figure 29. FCGR results on Al-4Li-1Cu-1Mg-0.2Zr, T851 temper: (○, ●) LT orientation, (△) TL orientation, and (---) typical results for 7075-T651 (16).

5.3.5 Corrosion Resistance

Weight-loss rates of the Al-4Li alloys, constantly immersed in 3.5% NaCl solution for 125 hr, are: Al-4Li-1Cu-1Mg-0.2Zr-T8, 0.059 mm/y; Al-4Li-0.5Cu-1.5Mg-0.2Zr-T8, 0.015 mm/y; and Al-4Li-1.5Cu-0.5Mg-0.2Zr-T8, 0.136 mm/y. These rates compare favorably with the 0.04-0.09 mm/y measured for 7075-T6 in natural seawater in 1-5 y tests. The corrosion resistance of Al-4Li alloys in salt solutions is naturally high and is lowered as the Cu:Mg ratio is increased.

5.4 Microstructure/Properties Correlation

Small additions of Cu and Mg to RSP Al-4Li cause the mutual [Li + Cu + Mg] solubility limit to be exceeded. Additions of 0.5-1.5 wt% Cu or Mg are insufficient to allow precipitation of phases other than δ'. The strengths of the three alloys studied here are fixed by the grain size and δ' concentration, and are independent of the Cu:Mg ratio. Alloys with Cu:Mg ratios > 1

form large, brittle Cu-rich constituent particles upon solution-treatment. These particles degrade ductility, particularly in the transverse direction. The combination of insoluble constituent particles, inclusions, and oxides provides the alloys with generally marginal ductility and low fracture toughness.

The fatigue resistance and corrosion resistance of Al-4Li alloys are superior to those of 7075-T651. Corrosion resistance is inversely related to the Cu concentration and is independent of the Li concentration, in agreement with previous work (10). The high Li concentrations do not degrade strength, fatigue resistance, or corrosion resistance, but may interact with other microstructural factors such as the unrecrystallized microstructure and oxide inclusions to lower ductility and fracture toughness. The potential of this alloy class can be evaluated completely only if powder production and processing can be improved to produce mill forms which have clean, inclusion-free microstructures. The most promising alloy for further development is Al-4Li-0.5Cu-1.5Mg-0.2Zr, which combines low density, reasonable strength, adequate ductility in the T8 temper, and high corrosion resistance.

6. CONCLUSIONS

1. RSP baseline and dispersoid-containing Al-3Cu-2Li-1Mg-0.2Zr alloys maintain peak-aged yield stresses ≥ 575 MPa and ultimate tensile stresses up to 650 MPa at test temperatures between 25 and 150°C.
2. Density-normalized yield stresses of RSP Al-3Cu-2Li-1Mg-0.2Zr alloys are up to 52% larger than that of 2124-T851, 30% larger than that of mill-annealed Ti-6Al-4V, and 10% larger than that of solution-treated-and-aged Ti-6Al-4V at 150°C. The RSP alloys are attractive substitutes for 2XXX aluminum alloys and high-strength titanium alloys in intermediate-temperature applications.
3. High strength in Al-3Cu-2Li-1Mg-0.2Zr alloys is provided between 25 and 150°C by thermally stable δ' (Al_3Li), T_1 (Al_2LiCu), and S' (Al_2CuMg) precipitates. [Fe + Ni]- and Cr-containing dispersoids in extrusions made from vacuum-atomized powders are too large to significantly improve strength in this temperature range.
4. The density-normalized yield stresses of RSP Al-3Cu-2Li-1Mg-0.2Zr alloys are up to 100% larger than that of 2124-T851 and equivalent to that of RSP Al-8Fe-4Ce at 260°C. The RSP alloys are attractive low-density substitutes for I/M and non-heat-treatable aluminum alloys for short (< 100-hr) exposures at this temperature.
5. Incorporation of 5 vol% Al_9FeNi or $\text{Al}_{18}\text{Cr}_2\text{Mg}_3$ dispersoids increases the yield stress of Al-3Cu-2Li-1Mg-0.2Zr by as much as 20% at 260°C. Sub-boundary constituent particles such as T_1 and S also contribute significantly to the strengths of these alloys above 150°C.
6. RSP Al-4Li-Cu-Mg-Zr alloys have ambient-temperature yield and ultimate tensile stresses similar to that of 7050-T7651, and are 14-14.5% less dense. The most promising of the three alloys investigated here is Al-4Li-0.5Cu-1.5Mg-0.2Zr because of its 20% higher density-normalized specific yield stress, 40% higher density-normalized elastic modulus, and superior corrosion resistance compared to the properties of 7050-T7651,

combined with adequate ductility. Al-4Li alloys containing ≥ 1 wt% Cu have coarse, brittle Cu-containing constituent particles and poor properties in the transverse orientation.

7. Additions of Cu and Mg to RSP Al-4Li are constrained by the [Li + Cu + Mg] solubility limit in the matrix. Usable Al-4Li-Cu-Mg-Zr alloys are strengthened by the substructure and δ' precipitates and not by Cu- or Mg-containing precipitates. Strength in the Al-4Li-Cu-Mg-Zr alloy class is independent of Cu:Mg ratio.
8. Fatigue-crack-growth rates of the Al-Li-Cu-Mg-Zr alloys investigated here are equal to or lower than that of 7075-T6, but inferior to that of 2124-T851.
9. The corrosion resistance of RSP Al-Li alloys in 3.5% NaCl solution is influenced most strongly by the Cu concentration, and is virtually independent of Li concentration up to 4 wt% Li.
10. Fracture toughnesses and transverse-orientation tensile properties are low in both alloy classes as a result of relatively high concentrations of oxide inclusions. These inclusions were probably formed in the melt prior to powder atomization. Improvements in melt practice such as in-line filtering, purification of the protective atmosphere, or substitution of less-reactive refractory crucibles are required to produce clean powders and consolidated forms having optimal properties.

7. REFERENCES

1. P. J. Meschter, R. J. Lederich, J. E. O'Neal, and P. S. Pao, Study on Effects of Powder and Flake Chemistry and Morphology on the Properties of Al-Cu-Mg-X-X-X Powder Metallurgy Advanced Aluminum Alloys, NASA Contractor Report 177946 (November 1985).
2. K. K. Sankaran, S. M. L. Sastry, and J. E. O'Neal, Microstructure and Deformation of Rapidly Solidified Al-3Li Alloys Containing Incoherent Dispersoids, in Aluminum-Lithium Alloys, T. H. Sanders, Jr. and E. A. Starke, Jr., eds. (TMS-AIME, Warrendale, PA, 1981), p. 189.
3. S. M. L. Sastry, P. J. Meschter, J. E. O'Neal, and K. K. Sankaran, Microstructure and Properties of Powder-Processed Aluminum-Lithium Alloys, McDonnell Douglas Report No. MDC Q0778 on AFOSR Contract No. F49620-79-C-0039 (May 1982).
4. K. K. Sankaran, J. E. O'Neal, and S. M. L. Sastry, Effects of Second-Phase Dispersoids on Deformation Behavior of Al-Li Alloys, Metallurgical Transactions 14A, 2174 (1983).
5. P. J. Meschter, J. E. O'Neal, and R. J. Lederich, Effect of the Rapid-Solidification Method on Microstructures and Properties of Al-Li Alloys, in Rapid Solidification Processing--Principles and Technologies, III, R. Mehrabian, ed., National Bureau of Standards, Washington, DC, 1983, p. 281.
6. P. J. Meschter, J. E. O'Neal, and R. J. Lederich, Effect of Rapid-Solidification Method on the Microstructure and Properties of Al-3Li-1.5Cu-0.5Co-0.2Zr, in Aluminum-Lithium Alloys II, T. H. Sanders, Jr. and E. A. Starke, Jr., eds. (TMS-AIME, Warrendale, PA, 1984), p. 419.
7. K. K. Sankaran and J. E. O'Neal, Structure-Property Relationships in Al-Cu-Li Alloys, in Aluminum-Lithium Alloys II, T. H. Sanders, Jr. and E. A. Starke, Jr., eds. (TMS-AIME, Warrendale, PA, 1984), p. 393.

8. P. J. Meschter, P. S. Pao, R. J. Lederich, and J. E. O'Neal, Effect of Compositional Variations on the Microstructures and Properties of Rapidly Solidified Al-3Li Alloys, in Rapidly Solidified Powder Aluminum Alloys, E. A. Starke, Jr. and M. Fine, eds. (ASTM, Philadelphia, PA 1986) p. 512.
9. P. J. Meschter, R. J. Lederich, and J. E. O'Neal, Rapid Solidification and P/M Processing of Aluminum-Lithium Alloys, in Modern Developments in Powder Metallurgy, Vol. 16, E. N. Aqua and C. I. Whitman, eds. (Metal Powder Industries Federation, American Powder Metallurgy Institute, Princeton, NJ, 1986) p. 437.
10. P. J. Meschter, R. J. Lederich, and J. E. O'Neal, Microstructure and Properties of Rapid Solidification Processed (RSP) Al-4Li and Al-5Li Alloys, in Aluminum-Lithium Alloys III, C. Baker, P. J. Gregson, S. J. Harris, and C. J. Peel, eds. (The Institute of Metals, London, 1986), p. 85.
11. Aluminum-Lithium Alloys, T. H. Sanders, Jr. and E. A. Starke, Jr., eds. (TMS-AIME, Warrendale, PA, 1981).
12. Aluminum-Lithium Alloys II, T. H. Sanders, Jr. and E. A. Starke, Jr., eds. (TMS-AIME, Warrendale, PA, 1984).
13. Aluminum-Lithium Alloys III, C. Baker, P. J. Gregson, S. J. Harris, and C. J. Peel, eds. (The Institute of Metals, London, 1986).
14. C. M. Adam and R. E. Lewis, High Performance Aluminum Alloys, in Rapidly Solidified Crystalline Alloys, S. K. Das, B. H. Kear, and C. M. Adam, eds. (TMS-AIME, Warrendale, PA, 1985), p.157.
15. Metals Handbook, Ninth Ed., Volume 3, Properties and Selection: Stainless Steels, Tool Materials, and Special-Purpose Materials (American Society for Metals, Metals Park, OH, 1980).

16. Metals Handbook, Ninth Ed., Volume 2, Properties and Selection: Nonferrous Alloys and Pure Metals (American Society for Metals, Metals Park, OH, 1979).
17. I. G. Palmer et al., in reference 12, p. 91.
18. I. G. Palmer, R. E. Lewis, and D. D. Crooks, in reference 11, p. 241.
19. M. W. Mahoney and C. H. Hamilton, Superplastic Aluminum Evaluation, Report No. AFWAL-TR-81-3051 (AD-A107760) on Air Force Contract No. F33615-79-C-3218 (June 1981).
20. L. F. Mondolfo, Aluminum Alloys: Structure and Properties (Butterworths, London, 1976).
21. R. E. Crooks and E. A. Starke, Jr., The Microstructure and Tensile Properties of a Splat-Quenched Al-Cu-Li-Mg-Zr Alloy, Metallurgical Transactions 15A, 1367 (1984).
22. J. A. Wert et al., Grain Refinement in 7075 Aluminum by Thermomechanical Processing, Metallurgical Transactions 12A, 1267 (1981).
23. R. E. Sanders, Jr. and G. J. Hildeman, Elevated Temperature Aluminum Alloy Development, Report No. AFWAL-TR-81-4076 on Air Force Contract No. F33615-77-C-5086 (September 1981).
24. W. M. Griffith, R. E. Sanders, Jr., and G. J. Hildeman, Elevated Temperature Aluminum Alloys for Aerospace Applications, in High-Strength Powder Metallurgy Aluminum Alloys, M. J. Koczak and G. J. Hildeman, eds. (TMS-AIME, Warrendale, PA, 1982), p. 209.
25. B. Noble, S. J. Harris, and K. Dinsdale, Yield Characteristics of Aluminum-Lithium Alloys, Metal Science 16, 425 (1982).
26. P. Sainfort and P. Guyot, Fundamental Aspects of Hardening in Al-Li Alloys, in reference 13, p. 420.

27. B. Noble, S. J. Harris, and K. Harlow, Mechanical Properties of Al-Li-Mg Alloys at Elevated Temperatures, in reference 12, p. 65.
28. S. M. L. Sastry and J. E. O'Neal, High-Temperature Deformation Behavior and Mechanical Properties of Rapidly Solidified Al-Li-Co and Al-Li-Zr Alloys, in reference 12, p. 79.
29. M. Pridham, B. Noble, and S. J. Harris, Elevated Temperature Strength of Al-Li-Cu-Mg Alloys, in reference 13, p. 547.
30. P. J. Meschter, R. J. Lederich, J. E. O'Neal, E. J. Lavernia, and N. J. Grant, Microstructure and Properties of Liquid-Dynamic Compacted Al-4Li-1Cu-0.2Zr, 115th TMS Annual Meeting, New Orleans, LA, 2-6 March 1986.
31. W. E. Quist, G. H. Narayanan, A. L. Wingert, and T. M. F. Ronald, Analysis of Powder Metallurgy and Related Techniques for the Production of Aluminum-Lithium Alloys, in reference 13, p. 625.
32. T. Malis, Characterization of Lithium Distribution in Aluminum Alloys, in reference 13, p. 347.
33. F. W. Gayle and J. B. Vandersande, $Al_3(Li,Zr)$ or α' Phase in Al-Li-Zr System, in reference 13, p. 376.
34. C. Sigli and J. M. Sanchez, Calculation of Phase Equilibrium in Al-Li Alloys, *Acta Metallurgica* 34, 1021 (1986).
35. J. M. Papazian, C. Sigli, and J. M. Sanchez, New Evidence for GP Zones in Binary Al-Li Alloys, *Scripta Metallurgica* 20, 201 (1986).

Standard Bibliographic Page

1. Report No. NASA CR-178145		2. Government Accession No.		3. Recipient's Catalog No.	
4. Title and Subtitle Study on Effects of Powder and Flake Chemistry and Morphology on the Properties of Al-Cu-Mg-x-x-x Powder Advanced Aluminum Alloys - Final Report				5. Report Date August 1986	
				6. Performing Organization Code	
7. Author(s) P. J. Meschter, R. J. Lederich, and J. E. O'Neal				8. Performing Organization Report No.	
				10. Work Unit No.	
9. Performing Organization Name and Address McDonnell Douglas Research Laboratories P.O. Box 516 St. Louis, MO 63166				11. Contract or Grant No. NAS1-17107	
				13. Type of Report and Period Covered Contractor Report	
12. Sponsoring Agency Name and Address National Aeronautics and Space Administration Langley Research Center Hampton, VA 23665				14. Sponsoring Agency Code	
				15. Supplementary Notes Langley Technical Monitor; W. Barry Lisagor Final Report	
16. Abstract A study was conducted (1) to develop RSP dispersoid-containing Al-3Cu-2Li-1Mg-0.2Zr alloys as substitutes for titanium alloys and commercial 2XXX aluminum alloys for service to at least 150°C, and (2) to develop RSP Al-4Li-Cu-Mg-Zr alloys as substitutes for high-strength commercial 7XXX alloys in ambient-temperature applications. RSP Al-3Cu-2Li-1Mg-0.2Zr alloys have density-normalized yield stresses at 150°C up to 52% larger than that of 2124-T851 and up to 30% larger than that of Ti-6Al-4V. Strength at 150°C in these alloys is provided by thermally stable δ' (Al ₃ Li), T ₁ (Al ₂ LiCu), and S' (Al ₂ CuMg) precipitates. Density-normalized yield stresses of RSP Al-3Cu-2Li-1Mg-0.2Zr alloys are up to 100% larger than that of 2124-T851 and equivalent to that of Al-8Fe-4Ce at 260°C. Strength in the RSP alloys at 260°C is provided by incoherent dispersoids and subboundary constituent particles such as T ₁ and S. The RSP alloys are attractive substitutes in < 100-h exposures for 2XXX and Al-Fe-Ce alloys up to 260°C and for titanium alloys up to 150°C. RSP Al-4Li-Cu-Mg-Zr alloys have ambient-temperature yield and ultimate tensile stresses similar to that of 7050-T7651, and are 14% less dense. RSP Al-4Li-0.5Cu-1.5Mg-0.2Zr has a 20% higher specific yield stress, 40% higher specific elastic modulus, and superior corrosion resistance compared to the properties of 7050-T7651. Strength in the Al-4Li-Cu-Mg-Zr alloy class is primarily provided by the substructure and δ' precipitates and is independent of Cu:Mg ratio. Improvements in fracture toughness and transverse-orientation properties in both alloy classes depend on improved melt practices to eliminate oxide inclusions which are incorporated into the consolidated forms.					
17. Key Words (Suggested by Authors(s)) Rapid solidification Aluminum-lithium alloys Consolidation Powder Metallurgy Extrusion			18. Distribution Statement Unclassified-unlimited		
19. Security Classif.(of this report) Unclassified		20. Security Classif.(of this page) Unclassified		21. No. of Pages 73	22. Price

End of Document